U.S. DEPARTMENT OF COMMERCE
National Technical Information Service

AD-A028 884

The Physics of Reliability of Future Electronic Devices

IBM Thomas J. Watson Research Center

May 1976

RADC-TR-76-180
Final Report
May 1976

ADA028884

THE PHYSICS OF RELIABILITY OF FUTURE ELECTRONIC DEVICES

IBM Thomas J. Watson Research Center

Approved for public release;
distribution unlimited.

Sponsored by
Defense Advanced Research Projects Agency
ARPA Order No. 2180

ROME AIR DEVELOPMENT CENTER
AIR FORCE SYSTEMS COMMAND
GRIFFISS AIR FORCE BASE, NEW YORK

REPRODUCED BY
NATIONAL TECHNICAL
INFORMATION SERVICE
U.S. DEPARTMENT OF COMMERCE
SPRINGFIELD, VA. 22161

DISCLAIMER NOTICE

THIS DOCUMENT IS THE BEST QUALITY AVAILABLE.

COPY FURNISHED CONTAINED A SIGNIFICANT NUMBER OF PAGES WHICH DO NOT REPRODUCE LEGIBLY.

ARPA Order No. 2180

Program Code No. 2D1

Contractor: IBM Corporation

Effective Date of Contract:
1 June 1974

Contract No. F19628-74-C-0C77

Co-Principal Investigator and Phone No.
Dr. Thomas H. DiStefano/914-945-22[illegible]
Dr. King-Ning Tu/914-945-1602

AFCRL Project Scientist and Phone No.
Dr. John C. Garth/617-861-4051

Contract Expiration Date: 30 November 1975

Qualified requestors may obtain addition copies from the Defense Documentation Center. All others should apply to the National Technical Information Service.

Unclassified

SECURITY CLASSIFICATION OF THIS PAGE (When Data Entered)

REPORT DOCUMENTATION PAGE

READ INSTRUCTIONS BEFORE COMPLETING FORM

1. REPORT NUMBER RADC-TR-76-160	2. GOVT ACCESSION NO.	3. RECIPIENT'S CATALOG NUMBER
4. TITLE (and Subtitle) THE PHYSICS OF RELIABILITY OF FUTURE ELECTRONIC DEVICES		5. TYPE OF REPORT & PERIOD COVERED Final Report 1Jun74 - 30Nov75
		6. PERFORMING ORG. REPORT NUMBER
7. AUTHOR(s) T. H. DiStefano, K. N. Tu		8. CONTRACT OR GRANT NUMBER(s) F19628-74-C-0077
9. PERFORMING ORGANIZATION NAME AND ADDRESS IBM Thomas J. Watson Research Center, International Business Machines Corporation, P. O. Box 218, Yorktown Heights, N.Y. 10598		10. PROGRAM ELEMENT, PROJECT, TASK AREA & WORK UNIT NUMBERS 61101D 56210905
11. CONTROLLING OFFICE NAME AND ADDRESS Deputy for Electronic Technology(RADC/ ETSR, Hanscom AFB, MA 01731, Contract Monitor: John C. Garth/ETSR		12. REPORT DATE May 1976
		13. NUMBER OF PAGES
14. MONITORING AGENCY NAME & ADDRESS(if different from Controlling Office)		15. SECURITY CLASS. (of this report) UNCLASSIFIED
		15a. DECLASSIFICATION/DOWNGRADING SCHEDULE

16. DISTRIBUTION STATEMENT (of this Report)

A- Approved for public release; distribution unlimited.

17. DISTRIBUTION STATEMENT (of the abstract entered in Block 20, if different from Report)

18. SUPPLEMENTARY NOTES

This research was supported by the Defense Advanced Research Projects Agency. ARPA Order No. 2180

19. KEY WORDS (Continue on reverse side if necessary and identify by block number)

Dielectric Breakdown, Optical Scanning, Silicon Surface Defects, Photovoltage, Schottky Barrier, Interfaces, Diffusion Marker, Insulators, Low Temperature Reaction, Back Scattering, Silicide

20. ABSTRACT (Continue on reverse side if necessary and identify by block number)

Among the major reliability problems in semiconductor devices are semiconductor surface defects, dielectric breakdown, interdiffusion across interfaces, and corrosion. In the area of surface defects, we have used scanned optical techniques to probe defects and recombination centers on silicon surfaces. Crystallographic defects on silicon surfaces, of the type measured by the scanned optical techniques SIP and SSP are known to promote device failure.

DD FORM 1 JAN 73 1473 EDITION OF 1 NOV 65 IS OBSOLETE

Unclassified

SECURITY CLASSIFICATION OF THIS PAGE (When Data Entered)

The problem of dielectric breakdown in SiO_2, which is particularly important to the reliability of integrated circuits, was investigated both theoretically and experimentally. A simple theory, based on impact ionization and a subsequent field distortion is able to explain thickness and electrode dependence of the process, as well as the radiation sensitivity of dielectric breakdown.

Interface reactions were found to be particularly important to the reliability of Schottky barriers. Several classifications of metals have been determined and studied with respect to their behavior in the formation of metal silicide Schottky barrier contacts to silicon. On the basis of the classification of reaction properties, the reaction between the metal and either silicon or SiO_2 can be explained and understood.

Table of Contents

Page

I. The Physics of Reliability of Future Electronic Devices 1

II. Dielectric Instability and Breakdown in SiO_2 Thin Films 5

III. Photoemission and Photovoltaic Imaging of Semiconducting Surfaces . 27

IV. The Electronic Structure of the Si - SiO_2 Interface 59

V. Interfacial Reactions in Solids 75

VI. Surface Reactions on MOS Structures 79

VII. Publications and Oral Presentations (F19628-73-C-0006 and F19628-74-C-0077) 97

ACCESSION for
NTIS White Section
DDC Buff Section
UNANNOUNCED
JUSTIFICATION
BY
DISTRIBUTION/AVAILABILITY CODES
Dist. AVAIL. and/or SPECIAL
A

THE PHYSICS OF RELIABILITY OF FUTURE ELECTRONIC DEVICES

I. SUMMARY OF THE RESEARCH PROGRAM

Interfaces between dissimilar materials have become an important part of modern electronic devices, particularly in the area of microelectronics, where materials such as semiconductors, metals and insulators are combined in order to use their unique properties and to achieve the high performance and small dimensions required in modern technology. The devices that will be important in the next decade are classified into several dominant technologies: silicon (MOS, I^2L, and bipolar), magnetic films and sensors, and superconducting films. Reliability problems in microminiature devices, such as those anticipated for the next decade, are frequently due to interface reactions, surface defects in the semiconductor, surface and grain boundary reactions, charging or breakdown in insulating films, and registration errors in lithography. The overall objective of our present work is to investigate the fundamental properties of interfaces between dissimilar materials that may influence the performance of future electronic devices, and to provide a scientific understanding of reliability problems associated with material interfaces in present devices. We concentrated on generic problems, both present and anticipated, for which an adequate scientific basis was lacking; short term problems pecular to any one specific device were not emphasized. The program, which was funded under ARPA Contract Nos. F19628-73-C-0006 and F19628-74-C-0077 for thirty-six months, was largely concerned with fundamental problems in MOS and bipolar silicon devices, although a few types of bipolar switches found in amorphous materials were investigated.

II. SIGNIFICANT RELIABILITY PROBLEMS

The significant reliability problems found in silicon devices, which will comprise the major technology for the next decade, can be grouped into a few general areas.

A. Local Defects in the Silicon Surface

1. Surface defects in silicon material cause a reduction both in reliability and in device process yield.

   a. Even a small defect density can cause problems in dense, large area chips.

   b. Dislocations, diffusion pipes, and precipitates can cause a long term degradation.

2. Serious defects can be introduced during processing steps.

   a. Heavy local diffusion or ion implantation produces defects.

   b. Thick oxide layers (oxide isolation) or other insulator layers cause surface stresses and defects.

B. Charging and Breakdown in Dielectric Films

1. Dielectric breakdown is a continuing problem, particularly in the thin (∿200Å) gate insulator in MOS devices being developed.

   a. Initial failure due to defects in the SiO_2.
   b. Time delayed breakdown, which may be related to interdiffusion of material.

2. A long-term buildup of charge in an insulating layer is caused by the injection of hot carriers into insulator where they are trapped.

C. Packaging and Corrosion

1. Metal film corrosion due to trace amounts of S of H_2O gas is significant.
2. Electromigration in thin metal films will be a continuing problem in fine line LSI logic circuitry.

D. Lithography

1. Mask registration and defects are a cause of both immediate and long term failure of LSI devices.
2. New technologies involving X-ray or electron beam photoresist exposure produce radiation damage.

E. Degradation of Contact Interfaces

1. Most of the Schottky Barriers involved in LSI silicon technology are subject to degradation due to interdiffusion of materials.
2. Small changes in the gate contact barrier of MOS devices causes both immediate and long term problems in newer technologies using thin gate insulators.

III. ACCOMPLISHMENTS OF THE PROGRAM - Several significant reliability problems were studied in order to provide a practical and scientific basis for handling the problems. Our work was successful in developing new methods of characterization and measurement; in formulating models of failure mechanisms; and in better characterizing materials, particularly insulators. The more significant results of the program are outlined.

A. Local Defects on Silicon Surfaces

1. A new type of scanned surface photovoltage measurement has been developed which will non-destructively detect and image surface defects in silicon at various stages of processing.

   a. The photovoltage system has been applied successfully to the evaluation of silicon starting material.

   b. The resolution has been increased to about 0.8 micron, on the basis of a theoretical understanding which we developed.

2. The scanned internal photoemission technique has been developed and used to find and determine the influence of local sodium and phosphorus deposits on the Si-SiO_2 interface.

B. Dielectric Breakdown in Thin Insulating Films

1. A complete model was formulated to describe the process of dielectric breakdown in SiO_2 thin films. This model is the first to describe consistently all of the available data.

   a. The model predicts a significant increase in dielectric strength for films less than 300Å thick.
   b. Dielectric breakdown induced by a small amount of ionizing radiation was found and explained in terms of the theory.

2. The uniformity and dielectric properties of thin SiO_2 films were improved by compaction of the film with a careful, controlled amount of ion irradiation, with a subsequent anneal step.
3. The electronic structures of SiO_2 and Si_3N_4, pieced together on the basis of ESCA, photoemission, and reflectivity measurements, provide a basis for understanding dielectric breakdown and other events in these materials.

C. Fundamentals and Degradation of the MNOS Transistor

1. The energy level responsible for charge or information storage was measured for the first time with the newly developed technique of photocapacitance spectroscopy.
2. Both the Si_3N_4 and the SiO_2 have been characterized by several optical and photoemission techniques.
3. A type of degradation of MNOS structures, observed directly by the scanned surface photovoltage technique, appears to be due to a buildup of nonlocal charge in the double insulator.

D. Schottky Barriers on Silicon

1. A class of metals was found which will decompose a thin layer of SiO_2 on silicon at high temperatures to form a silicon-silicide Schottky barrier.

   a. A new technique of using an ion implanted Xe marker was used to study interdiffusion at the interface.
   b. Metals with a high heat of formation for both the silicide and the oxide phase were found to decompose SiO_2 at low temperatures. Integrated circuits using these metals are expected to exhibit long term failure.

E. Interface Polarization and Degradation

1. The interdiffusion of a metal into SiO_2 was studied by the new technique of field dependent photoemission. The resulting polarization layer can shift the operating point of an MOS device by several tenths of a volt over the life of the device (for particular gate metallizations such as gold, platinum, and others).

2. A small amount of hydrogen was found to produce an atomic polarization layer between SiO_2 and a catalytic metal such as platinum of palladium. This layer can shift the operating point of an MOS transistor by as much as 0.5 volt for certain gate metals. However, aluminum gates were found to be insensitive to hydrogen.

F. Metal - Glass Interaction

1. Phosphorus, a common dopant in glass, was found to crystallize glass at temperatures below those used in device processing. This reaction can cause a serious mode of failure in MOS circuits in which phosphorus is used to dope the SiO_2 gate insulator.
2. The adhesion between certain metals and glass was found to be greatly enhanced by the addition of a small amount of free silicon to the metal. This allows the use of gold on SiO_2, a combination which is normally not used because of poor adhesion.

II. DIELECTRIC INSTABILITY AND BREAKDOWN IN SiO_2 THIN FILMS*

by

T. H. DiStefano

IBM Thomas J. Watson Research Center

Yorktown Heights, New York 10598

and

M. Shatzkes

IBM System Products Division

Hopewell Junction, New York 12533

ABSTRACT

Dielectric instability and breakdown in SiO_2 have been well characterized by many experimental techniques, including measurements of thickness dependence, contact barrier dependence, and time dependence of breakdown as well as determination of radiation sensitivity and pre-breakdown charge buildup within the insulator. All of the various types of data can be explained consistently by an impact ionization model which predicts a negative resistance type of instability; electrons are injected from the cathode, the electron distribution is heated, hot electrons ionize the lattice, and the residual positive charge distorts the electric field to further increase impact ionization. The model is sensitive to two key parameters, the ionization bandgap E_g and the electron-phonon scattering length λ.

* Work supported in part by the Defense Advance Research Projects Agency and monitored by AFCRL under Contract No. F19628-74-C-0077.

I. INTRODUCTION

Although dielectric breakdown has been studied extensively for several decades[1-4], the events which occur during the incipient breakdown process in insulators are not completely understood. In the development of semiconductor technology, dielectric instability and breakdown in insulators such as SiO_2 have become increasingly significant in limiting both performance and reliability. Because of the importance of insulating thin films of SiO_2 in the integrated circuit industry, and because of the new information availabel on the properties of this material, it is fruitful to reexamine the physical processes which occur at high electric fields in order to gain insight into the possible intrinsic breakdown mechanisms. Reliable data is available on the dependence of breakdown upon insulator thickness, electrode work function,[5] and ionizing radiation[6] as well as on several material parameters of SiO_2 including ionization rate,[7] effective hole mobility,[8] and recombination cross section.[9] The problem of sorting out the details of the breakdown process in SiO_2 is considerably easier than in the traditional alkali halides due to the higher development of materials technology as well as the wealth of data on electronic properties which has become available for SiO_2. The fundamental phenomena which occur during intrinsic dielectric breakdown in thin films of SiO_2 can be explained and understood in a way that is consistent with all available data.

Historically, dielectric breakdown in insulators was first seen as an electronic avalanche process,[2, 3, 10-13] in which the field is high enough that one initial electron produces a destructively large cascade of ionizing events. The avalanche theories were able to explain the relatively

meager data available at the time, largely on the breakdown strength of alkali halide crystals. However, the significance of the phenomenon of field distortion[14] during breakdown was not appreciated until the proposal of a model by O'Dwyer who included the effect of the hole charge produced during the initial stages of an avalanche[15]. O'Dwyer was able to predict a negative resistance type of instability[15,16] in which electrons are injected from a cathode electrode by a field enhanced process, a portion of the electrons are accelerated sufficiently to produce impact ionization, and the slow moving holes left behind cause an enhancement of the cathode field which leads to an increased injection current, and so on, ad infinitum. The negative resistance in this model results from the nonlocal feedback produced by the drift of holes to the cathode. The O'Dwyer model resolves several deficiencies of the simple avalanche theories in that it explains why a low rate of avalanche multiplication is measured in insulators[7,17,18] near the breakdown field and it predicts a negative resistance type of instability which is impossible in a simple avalanche model. Further refinements[19,20] in the O'Dwyer model were made to account for the local details in the initial stages of breakdown. The O'Dwyer model characterizes breakdown quite well in semiconductors and in selected insulators, but it cannot be applied directly to insulators such as SiO_2 in which hole mobility is extremely small;[7,8] holes produced by impact ionization in SiO_2 are removed predominantly by recombination in the insulator leading to dielectric breakdown.

We have proposed[21] and explored a simple model based on impact ionization and field distortion that is appropriate to describe breakdown in

SiO_2, in which holes are relatively immobile. All of the physically significant processes are shown schematically in Fig. 1. Electrons are injected by field enhanced emission from a cathode, accelerated in the electric field, and scattered by phonon emission. A small fraction of these electrons create hole-electron pairs when they reach the ionization energy at approximately twice the bandgap Eg = 9.0 eV[23], leaving behind a cloud of relatively slow moving positive charge.[24] Holes are removed largely by recombination, with hole drift apparently playing only a minor role in the breakdown event. The net positive charge cloud leads to a larger current of more energetic electrons. As result, a negative resistance instability develops; in this case a position dependent ionization rate is necessary to provide the nonlocal feedback essential for negative resistance. The two principal differences between the proposed theory and that of O'Dwyer[24] are the dominance of recombination in removing holes from the charge cloud and the inclusion of a non-local rate of impact ionization. Although physical reality lies somewhere between the two extremes of hole annihilation by recombination and removal by drift, we find that the model based on recombination best describes the breakdown process in SiO_2. The impact ionization-recombination model[21,22,25], based on the most recent experimentally determined material parameters, is able to explain thickness, electrode, and radiation dependence of dielectic breakdown in thin films of SiO_2. The model is sensitive to only two key parameters, the bandgap of the insulator and the electron-phonon scattering length. Hole mobility is found to be an insignificant factor in the calculated dielectric strength for mobilities less than about 10^{-8} cm^2/V-sec.

II. IMPACT IONIZATION - RECOMBINATION MODEL

A model calculation based on steady state impact ionization and recombination is used to determine the J-V characteristic of a thin film of SiO_2. Dielectric breakdown occurs at the critical point at the onset of negative resistance, where dV/dJ =0. Electron current is injected from the cathode electrode into the SiO_2 by the strongly field dependent process of Fowler-Nordheim tunneling.[26] The injected electrons gain energy from the field and lose it to the lattice, primarily by phonon emission. In developing a nonlocal rate of impact ionization, it is assumed that a one dimensional projection of the electron-phonon scattering events is a Poisson process in which the probability of emitting a phonon is $(1/\lambda)$ per unit length in the X direction. The λ in this model is assumed to be energy independent.[27] In each phonon emission event, the electron loses a quantum of energy which is assumed to be that of an LO phonon for which $\hbar\omega$ = .153 eV.[28]

Based on the Poisson model, the electron energy distribution is found as a function of distance from the cathode. This distribution is then obtained in terms of a single adjustable parameter λ. The probability that a given electron will have energy $\varepsilon = -n\hbar\omega$ as it passes the point x is P, where

$$P(\varepsilon,x) = \frac{1}{(-\varepsilon/\hbar\omega)!} \left(\frac{x}{\lambda}\right)^{-\varepsilon/\hbar\omega} e^{-x/\lambda} .$$

By the central limit theorem, the energy distribution is approximately a Gaussian,

$$D(\varepsilon,x) \cong \frac{(1/\hbar\omega)}{[2\pi(x/\lambda)]1/2} \exp - \left\{\frac{[(\hbar\omega x/\lambda)-\varepsilon)]^2}{(\hbar\omega)^2(2x/\lambda)}\right\} .$$

We allow the electron to ionize the lattice as soon as it attains an energy of ε_i above the conduction band bottom; the rate of impact ionization is then

$$\left.\frac{\partial\rho_+}{\partial t}\right|_i = J\frac{\partial}{\partial x}\int_{\phi(x)+\varepsilon_i}^{0} D(\varepsilon,x)d\varepsilon,$$

where $\phi(x)$ is the energy at the bottom of the conduction band. In equilibrium, the rate of generation of holes equals that for hole recombination,

$$-\left.\frac{\partial\rho_+}{\partial t}\right|_r = \frac{J\rho_+}{e}\int_{\phi(x)}^{0} \sigma(\varepsilon)D(\varepsilon,x)d\varepsilon ,$$

where $\sigma(\varepsilon)$ is the recombination cross section. The equilibrium charge density is independent of the injected current J,

$$\rho_+ = \frac{e}{\langle\sigma\rangle}\frac{\partial}{\partial x}\int_{\phi(x)+\varepsilon_i}^{0} D(\varepsilon,x)d\varepsilon ,$$

where $\langle\sigma\rangle$ is the weighted average recombination cross section. The potential $\phi(x)$ is then found by a double numerical integration of Poisson's equation with an initial cathode field (or injected current) as a boundary condition.

The material parameters used in the calculation for SiO_2 are the phonon energy $\hbar\omega = .153$eV, $\epsilon = 3.8$, and the bandgap[23] $\varepsilon_g = 9$eV. There is considerable range of recombination cross section[29-33] found in SiO_2; the most recent evidence[33] indicates that a coulomb capture cross section is reasonable for the case of electron recombination with a trapped hole. The model calculations were based on a cross section,[34]

$$\sigma(\varepsilon) = \frac{1}{\pi}\left(\frac{3e^2}{16\varepsilon\varepsilon_o E}\right)^2 ,$$

which is $2.5 \times 10^{-13} cm^2$ at the electron saturation velocity in SiO_2. This $\sigma(\varepsilon)$, which is considerably larger than the direct radiative cross section used by the authors in a previous calculation,[22] provides a better fit to the available experimental data. A further refinement in the estimate of $\sigma(\varepsilon)$, to account for the effect of the electric field upon coulomb capture, may allow an even better fit. Fortunately, the model calculation is quite insensitive to details of the recombination coefficient, so that the predicted breakdown behavior is little influenced by the choice of capture cross section.

The electron-phonon scattering length λ is a critical parameter of the model; the calculated dielectic strength varies inversely with small changes in λ.[22] The value $\lambda = 1.74Å$ was chosen to fix the calculated breakdown voltage to $V_b = 92.5$ V for a 1000 Å thick film, in agreement with the available experimental data.[35-39] Then, the voltage at which dielectric breakdown takes place for a given thickness of SiO_2 is found from the critical point at which $dV/dJ=0$.

III. RESULTS

The ionization-recombination model was used to calculate J-V relationships and dielectric strength for a range of film thickness and contact barriers. The results for $\lambda = 1.74$ Å are compared with the experimental data presently available. Also, the results of an O'Dwyer type of model

calculation are given for a reasonable choice of parameters;[40] the mobility product $\mu_+\mu_-$ was set to fix the breakdown voltage V_{10} = 92.5V at 1000 Å. The thickness dependence of the measured dielectric strength is shown in Fig. 2, along with that calculated on the basis of our ionization-recombination model (solid curve) and O'Dwyer's model (dashed curve). The sharp rise in the experimentally determined breakdown strength[36,38] for thickness below ∿400 Å is well explained by the ionization-recombination model. The reason for this increase is the nonlocal ionization rate necessary in the ionization-recombination model; no ionization is possible for a region within $x_o = (\varepsilon_i + \Phi)/E$ of the cathode. Since our model predicts no intrinsic breakdown for voltages less than $(\varepsilon_i + \Phi)$ or ∿12 volts, the dielectric strength increases for small thickness as the breakdown voltage assymptotically approaches ∿12 V at an infinitesimally small thickness. On the other hand, the O'Dwyer type of model shows only a logarithmic dependence upon thickness, in part reflecting the use of a local ionization rate. Presumably, the use of nonlocal ionization would introduce a stronger thickness dependence into the model.

The experimentally determined breakdown strength[5] shows no systematic dependence upon the cathode contact barrier Φ as seen in Fig. 3. Here, the experimental uncertainty in each point is of the order of $\pm$ 0.5 x 10^6 V/cm. The calculated dielectric strength based on our ionization-recombination model shows a very weak dependence on the barrier Φ, in agreement with the general trend of the experimental findings. In contrast, the calculation based on an O'Dwyer type of model shows a strong dependence on Φ at the injecting contact. This difference in the barrier dependence of the two

theories results directly from the mechanism of clearing holes from the insulator. Based on the data available, it seems that recombination is the dominant mechanism in SiO_2. More definitive measurements of the barrier height dependence should enable a better determination of the role of hole mobility in the breakdown process.

Although electron-hole recombination appears to be the dominant mechanism of clearing holes from the SiO_2, hole motion may play a part in the breakdown process. In order to determine the influence of hole motion on our ionization-recombination model, the calculation was extended to allow holes to drift toward the cathode before recombining with injected electrons[41]. The nonlocal ionization rate was maintained, with $\lambda = 1.74$ Å. The results, shown in Fig. 4, show that dielectric strength is relatively unaffected by hole mobility up to $\sim 10^{-8}$ cm^2/V-sec. For the range of hole mobility reported[7,8] for SiO_2, the breakdown process and dielectric strength are little influenced by hole motion.

Based on the ionization-recombination model of the breakdown process in SiO_2, we would expect a stable charge cloud to form at fields below that at which breakdown takes place. Recently Shatzkes and Av-ron[42] have been able to measure this charge Q and its centroid $\bar{X}$; they used a combination of field emission and C-V measurements, performed at low field, to determine the remnant charge left from a previous high field pulse. The results are shown in Figures 5 and 6, for SiO_2 films of thickness 263 A and 493 A. The charge Q and centroid $\bar{X}$ calculated on the basis of the ionization-recombination model for 1000 Å of SiO_2 are shown as the solid curves in the two figures. The reasonably good overall agreement with experiment indicates

the existance of a stable charge cloud which behaves in a way predicted by the ionization-recombination theory.

IV. DISCUSSION

The impact ionization-recombination model for dielectric breakdown seem to be in reasonably good agreement with available data for SiO_2. From the model, a picture can be formulated of the significant processes which occur during breakdown. As shown in Fig. 7 the electrons are field emitted into the SiO_2 from the cathode electrode. The hottest of the electrons ionize the lattice, leaving behind slow moving holes. A cloud of positive charge formed by ionization and recombination leads to an increased current of hotter electrons. The result is that a negative resistance resistance type of instability develops in which a local charge cloud leads to an enhanced current. The small filament of current drains charge from the capacitor in a destructive breakdown event.

A nonlocal ionization rate is an essential feature of any model of dielectric breakdown in very thin insulating films. The influence of the nonlocal ionization rate is manifested in the rapid increase of the breakdown field seen in SiO_2 as the film thickness is reduced below about 400 Å. It is hardly surprising that a nonlocal ionization rate is important in films of a total thickness only several times greater than the distance required to accelerate a free electron up to the ionization energy.

During the electronic breakdown process, the experimental evidence indicates that recombination is the most important mode of removing holes produced by impact ionization. Hole drift to the cathode plays a relatively

minor role in determining the conditions leading to dielectric breakdown. One piece of experimental evidence, the dependence of dielectric strength on the cathode contact barrier, shows no systematic variation which would be expected if drift were the dominant mechanism of clearing holes from the insulator. Further, an impact ionization model calculation which includes both hole recombination and hole drift shows no appreciable influence on the dielectric strength for hole mobility $\mu < 10^{-8}$ cm^2/V-sec. Although hole mobility does not appear to have a significant effect on dielectric strength, it is thought to play a role in dielectric instability, particularly that induced by ionizing radiation of various sorts.

V. ACKNOWLEDGEMENT

The authors wish to acknowledge A. A. Levi for the numerical computation involved in the model and M. Av-ron for use of his unpublished data.

REFERENCES

1. N. Klein, Advances in Electronics and Electron Physics 26, 309 (1971)

2. W. Franz, im Handbuch der Physik, (S. Flugge, ed., Springer, Berlin 1956), Vol. XVII, p. 155.

3. R. Stratton, Prog. Dielectrics 3, 235 (1967).

4. J. J. O'Dwyer, The Theory of Dielectric Breakdown in Solids, (Oxford University Press, London, 1964).

5. C. M. Osburn and E. J. Weitzman, J. Electrochem. Soc. 119, 603 (1972).

6. T. H. DiStefano and P. K. Roy, The Physics of Interface Interaction Related to Reliability of Future Electronic Devices, Rept. No. AFCRL-TR-74-0263, available from Air Force Cambridge Laboratories, Bedford, Massachusetts.

7. P. Soloman, PhD Thesis, Technion (1974).

8. R. C. Hughes, Appl. Phys. Lett. 26, 436 (1975).

9. T. H. Ning, C. M. Osburn, and H. N. Yu, Appl. Phys. Lett. 26, 248 (1975).

10. H. Froelich, Proc. Roy. Soc. A160, 230 (1937); A188, 521 (1937); Rept. Prog. Phys. 6, 411 (1939).

11. A. von Hippel, J. Appl. Phys. 8, 815 (1937); Phys. Rev, 54, 1096 (1938).

12. F. Seitz, Phys. Rev. 76, 1376 (1949).

13. H. Callen, Phys. Rev. 76, 1394 (1949).

14. J. J. O'Dwyer, J. Appl. Phys. 37, 599 (1966).

15. J. J. O'Dwyer, J. Phys. Chem. Solids 28, 1137 (1967).

16. J. J. O'Dwyer, J. Appl. Phys. 40, 3887 (1969).

17. R. Williams, Phys. Rev. 125, 850 (1962).

18. N. Klein, private communication (1974).

19. N. Klein, Adv. Phys., 21, 605 (1972).

20. F. Forlani and N. Minnaja, Phys. Status Solidi 4, 311 (1964).

21. T. H. DeStefano and M. Shatzkes, Appl. Phys. Lett. 25, 685 (1974).

22. T. H. DeStefano and M. Shatzkes, Vac. Sci. Technol. 12, 37 (1975.

23. T. H. DiStefano and D. E. Eastman, Solid State Commun. 9, 2259 (1971).

24. It can be shown that the O'Dwyer model can be applied to the case of SiO_2 if the model parameters are appropriately chosen. In a previous article, the authors (ref.22) were unable to find a negative resistance for the case of an infinetisimally small ionization rate because of an improper choice of cathode condition.

25. M. Shatzkes, M. Av-ron, and R. M. Anderson, J. Appl. Phys. 45, 2065 (1974).

26. M. Lenzlinger and E. H. Snow, J. Appl. Phys. 40, 278 (1969).

27. G. A. Baraff, Phys. Rev. 128, 2507 (1962).

28. W. T. Lynch, J. Appl. Phys. 43, 3274 (1972).

29. R. Williams, Phys. Rev. 140, A569 (1965).

30. E. H. Nicolian, C. N. Berglund, P. F. Schmidt, and J. M. Andrews, J. Appl. Phys. 42, 5654 (1971).

31. D. J. DiMaria, PhD thesis (Lehigh University, 1973)

32. T. H. Ning and H. N. Yu, J. Appl. Phys. 45, 5373 (1974)

33. T. H. Ning, C. M. Osburn, and H. N. Yu, Appl. Phys. Lett. 26, 248 (1975).

34. A. Rose, Concepts in Photoconductivity and Allied Problems, (Interscience, New York, 1963) p. 121.

35. J. R. Ligenza, M. Kuhn, and A. D. Lopez, 138th Meeting of the Electrochem. Soc., Atlantic City, October 4-8, 1970.

36. C. M. Osburn, and D. W. Ormond, J. Electrochem. Soc. 119, 597 (1972).

37. N. J. Chou and J. M. Eldridge, J. Electochem. Soc. 117, 1288 (1970)

38. Kuniyuki Hamano, Jap. J. Appl. Phys. 13, 1085 (1974).

39. N. Klein, J. Electrochem. Soc. 116, 963 (1969).

40. The parameters used in the O'Dwyer model calculation are $H = 1.8 \times 10^8$ V/cm, $b = 2.2 \times 10^{19}$ sec^{-1} (from P. Solomon, ref. 7); and J (E) for Fowler-Nordheim tunneling from Si into SiO_2 (ref. 26). The mobility product $\mu_+\mu_-$ was determined by setting the breakdown voltage to $V_b = 92.5$ V at 1000 Å film thickness.

41. Details of this calculation are to be published elsewhere.

42. M. Shatzkes and M. Av-ron, to be published.

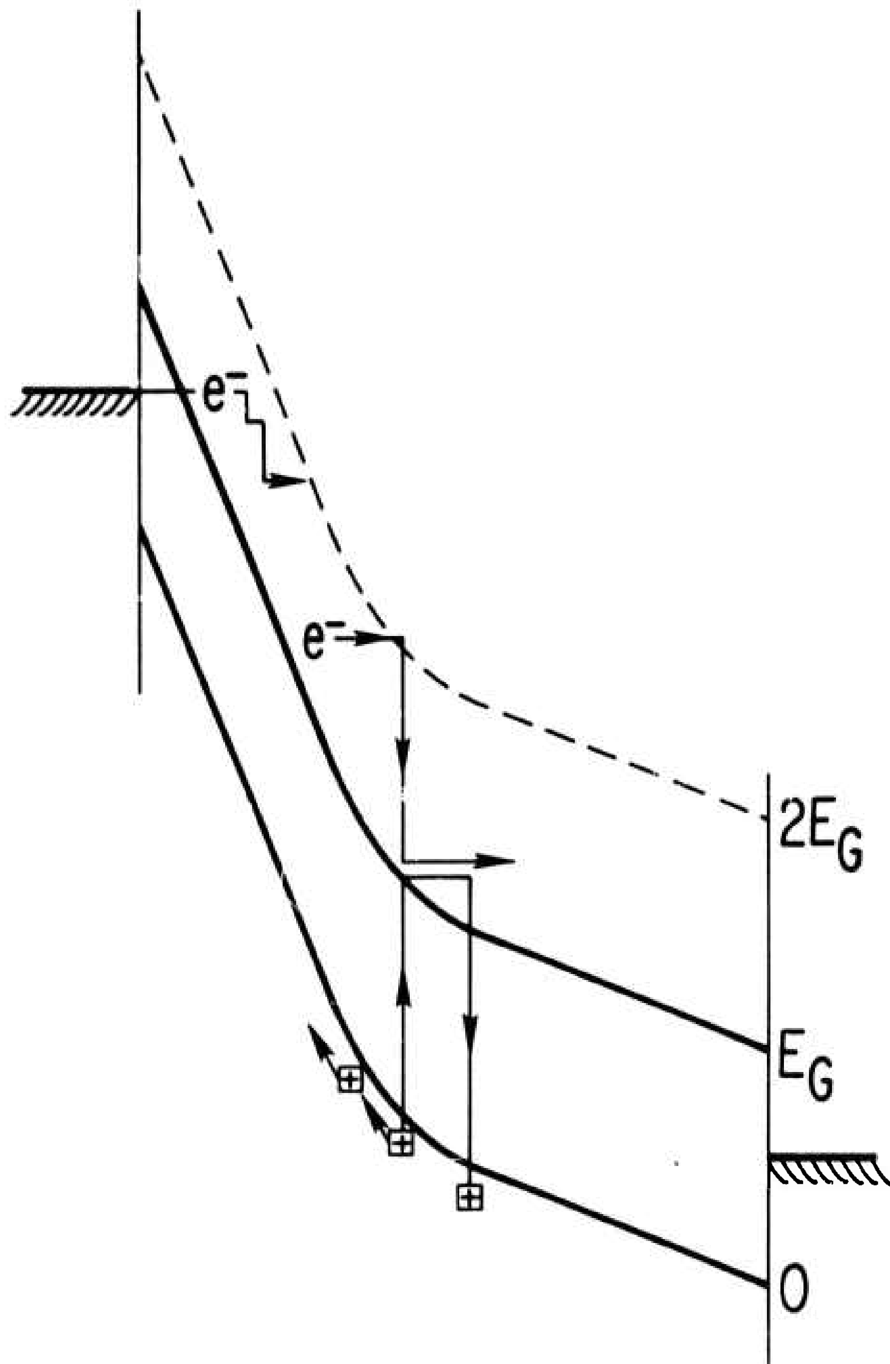

Figure 1. The physically important processes which occur in a thin film of SiO_2 at a high electric field. Electrons are injected by a field enhanced process at the cathode electrode. Hot electrons produce holes which induce a distortion of the electric field. Holes are removed predominantly by recombination and by drift to the cathode.

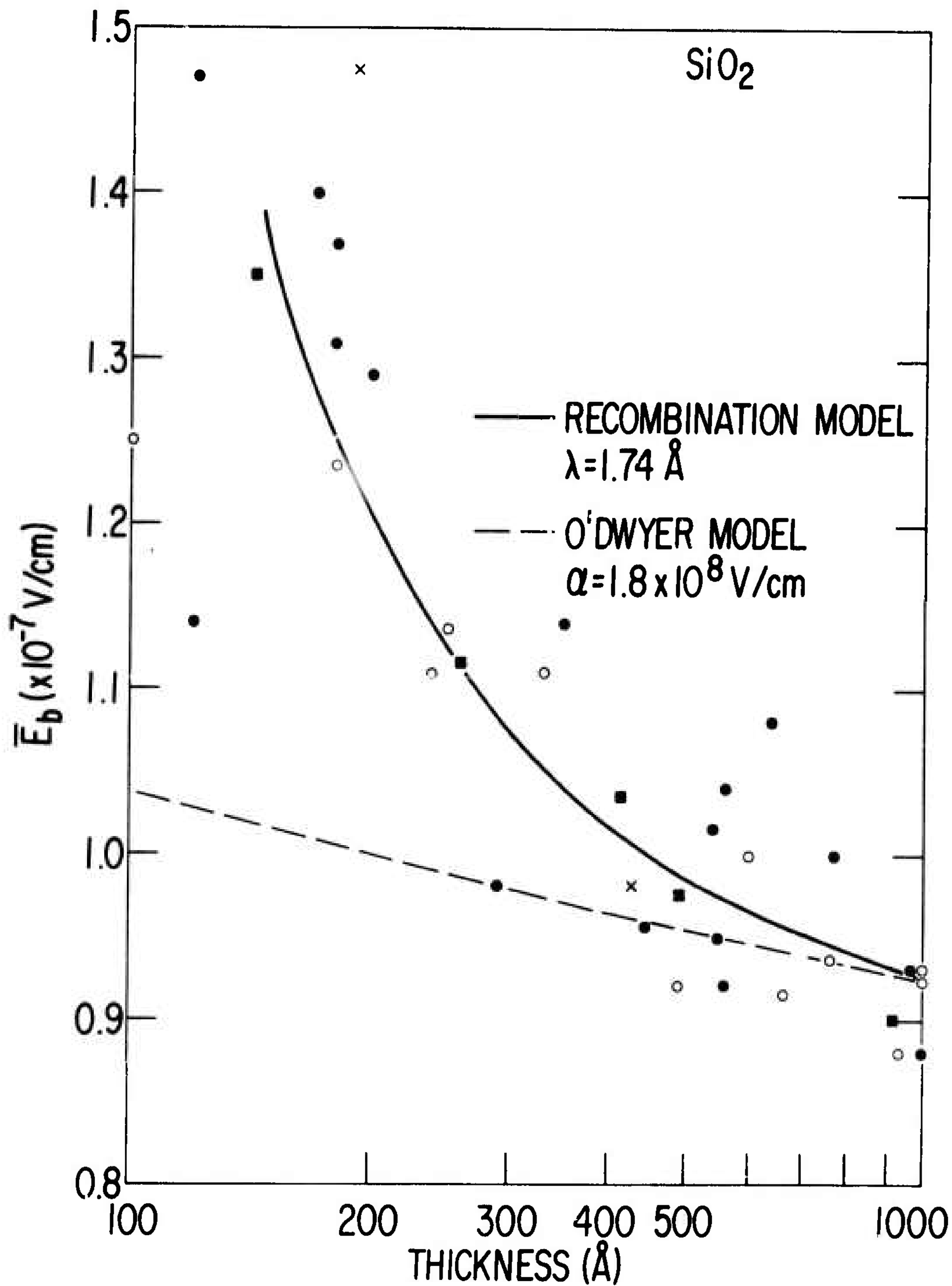

Figure 2. Dielectric strength as a function of thickness of an SiO_2 layer. The solid curve shows the results of our impact ionization-recombination theory for λ = 174 Å. The dashed curve is the calculated dielectric strength based on the O'Dwyer model, for a reasonable set of parameters (ref. 40). The best available experimental data on intrinsic breakdown is represented by the points: ■ Si(p)-SiO_2-Al; ● Si(n)-SiO_2-Al (ref. 36); O Si(p)-SiO_2-Al (ref.36); X K. Hamano (ref.38).

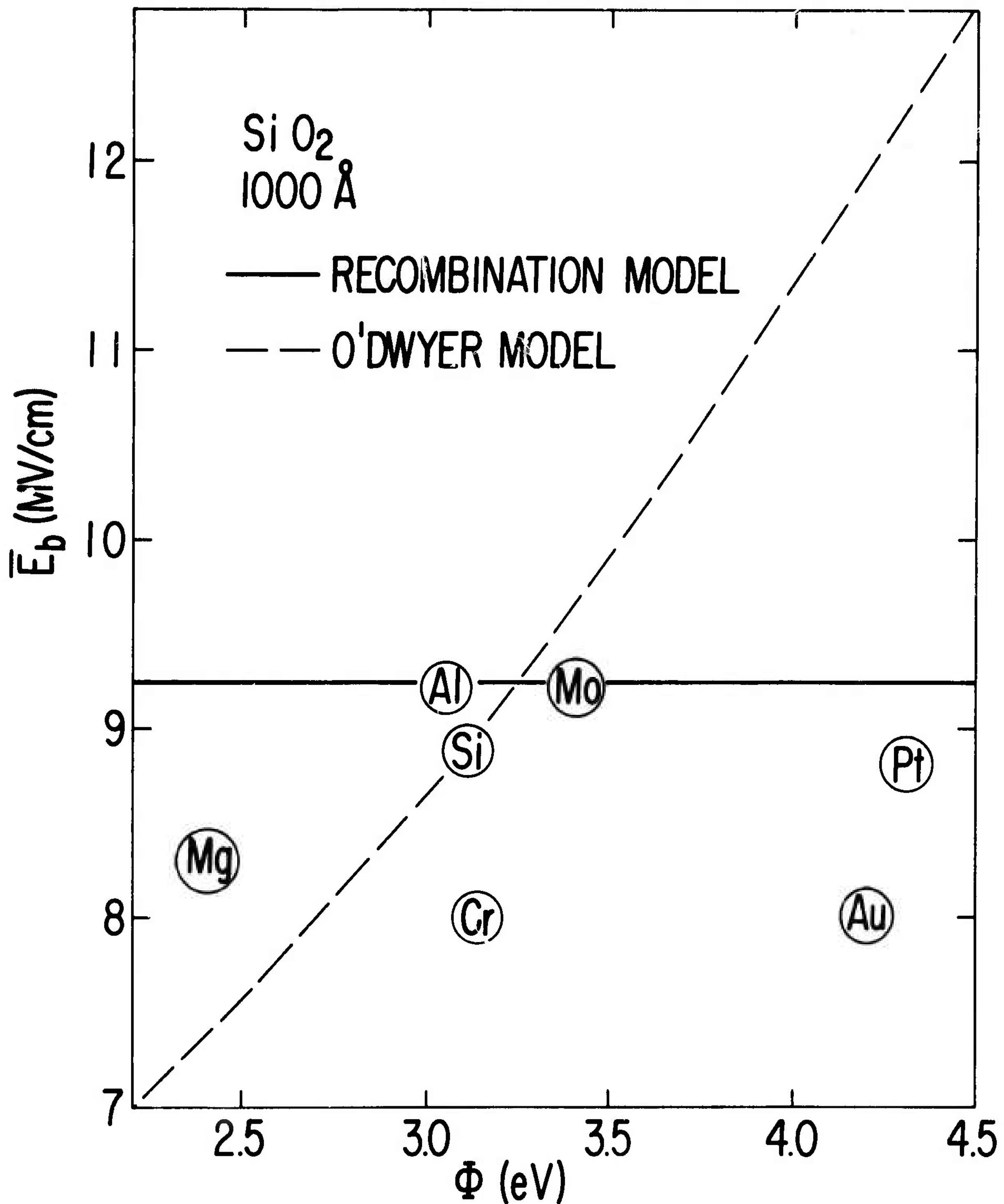

Figure 3. Dielectric strength as a function of cathode contact barrier Φ. The points shown for several metals, determined experimentally by Osburn and Weitzman (ref.5), are only approximate.

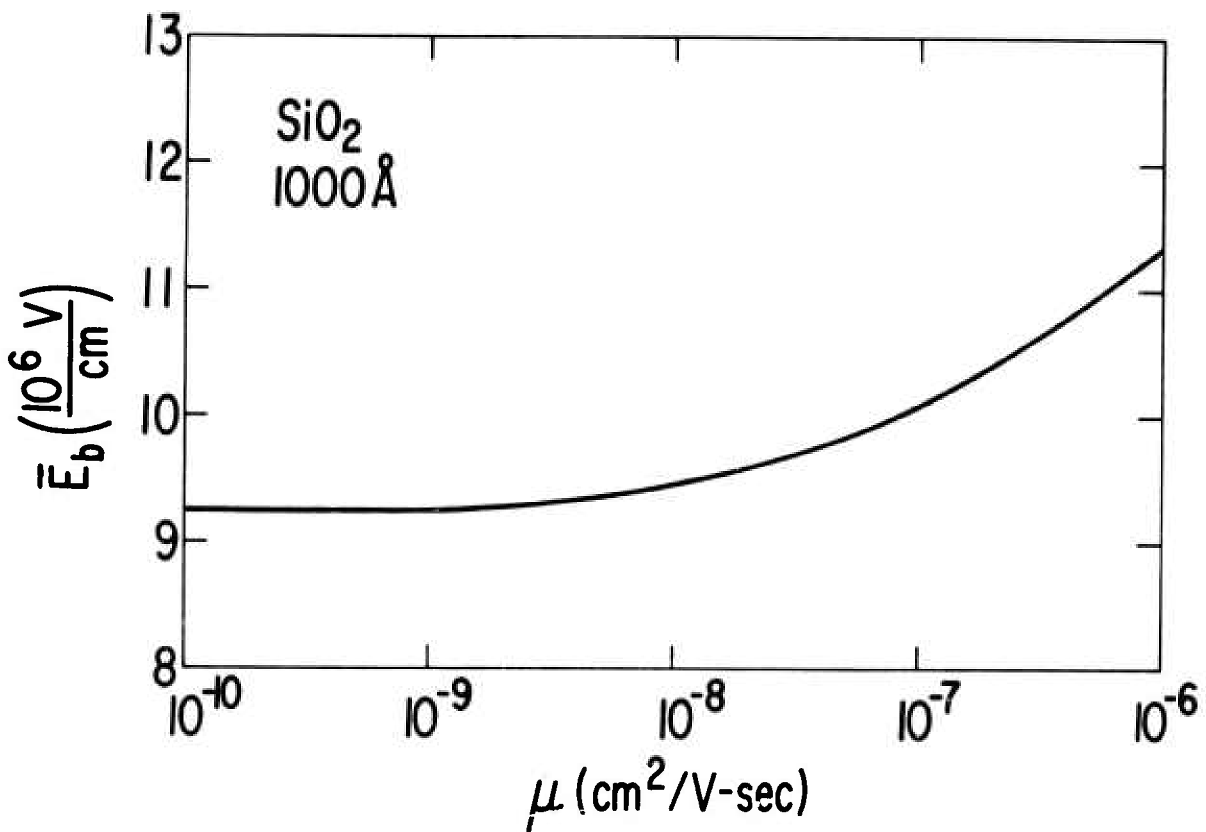

Figure 4. Dielectric strength calculated as a function of hole mobility for a model incorporating both recombination and hole mobility as mechanisms of clearing holes from the SiO_2.

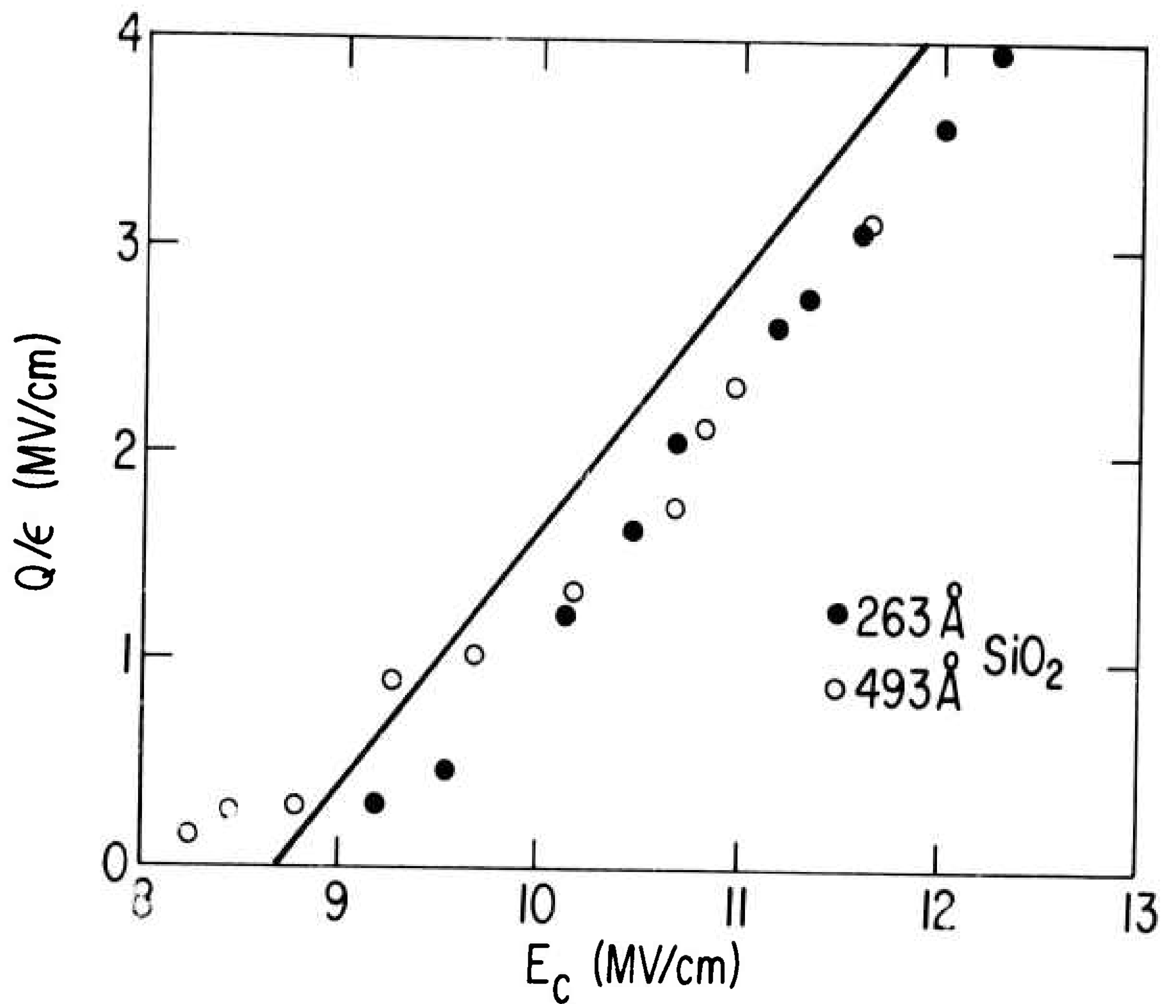

Figure 5. The total remnant charge density Q produced in the positive charge cloud in SiO_2 by a cathode field E_c. The solid curve is the calculated charge density in the ionization-recombination model with λ = 174 Å. The experimental points are from Shatzkes and Av-ron (ref.42).

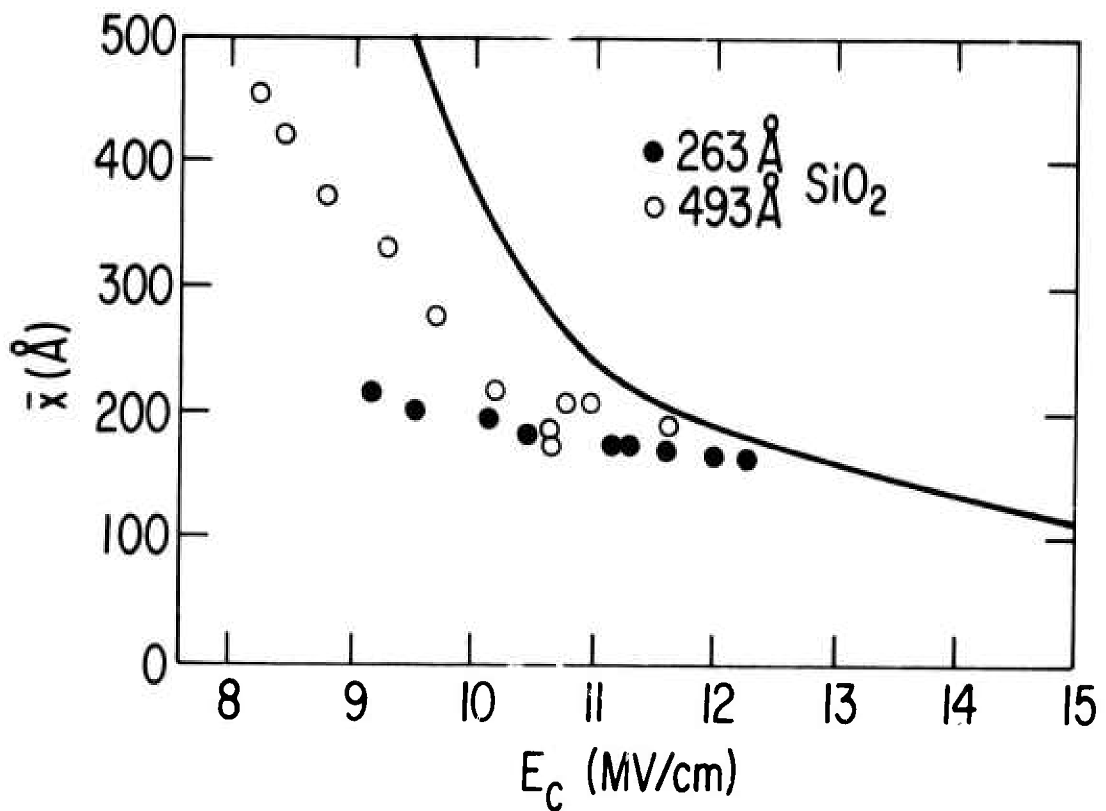

Figure 6. The centroid $\bar{X}$ of the charge cloud left in SiO_2 by a high electric field as a function of the electrode field E_c. The solid curve is the centroid calculated on the basis of the ionization-recombination model with $\lambda = 1.74$ Å. The experimental points are from Shatzkes and Av-ron (ref. 42).

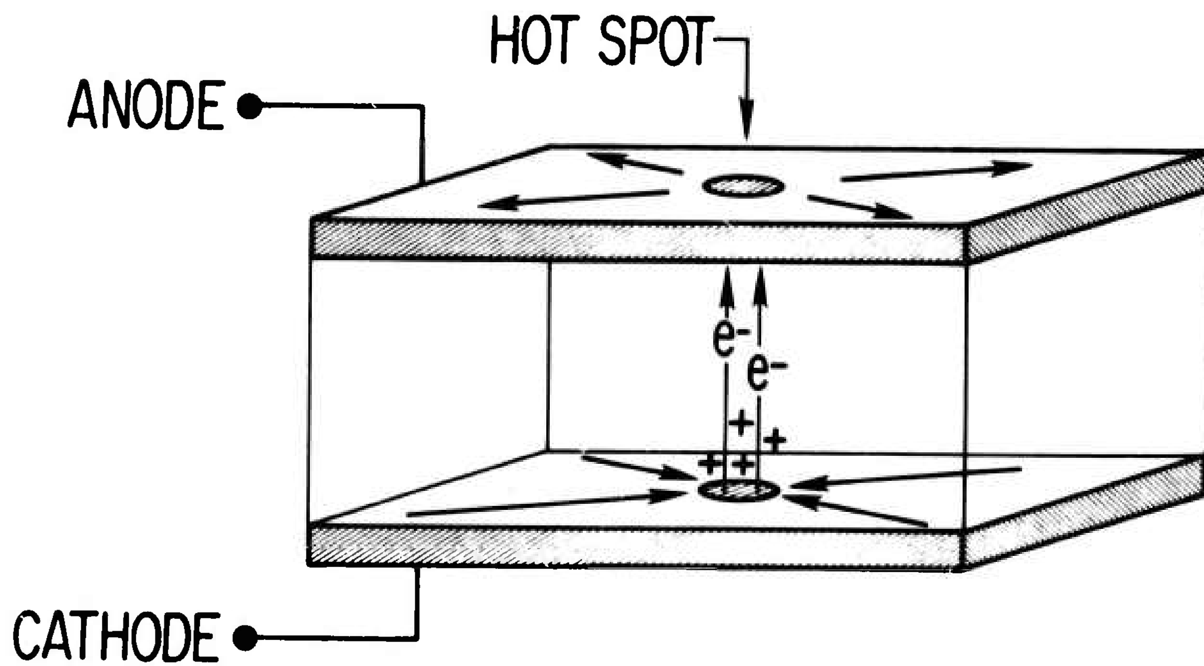

Figure 7. Schematic representation of the processes which occur during the critical stages of a dielectric breakdown in SiO_2.

III. PHOTOEMISSION AND PHOTOVOLTAIC IMAGING OF SEMICONDUCTOR SURFACES*

by

T. H. DiStefano

IBM Thomas J. Watson Research Center
Yorktown Heights, New York 10598

ABSTRACT: The new electro-optical techniques of scanned internal photoemission and scanned surface photovoltage can be used to obtain images of non-uniformities and defects at semiconductor surfaces or interfaces. The spatial resolution of either method is primarily determined by the wavelength of the laser used as a collimated light source. The images obtained by the photoemission technique are replicas of the local contact barrier at the interface between two materials. Typically, photoemission images show details due to variations of stoichiometry or local concentration of impurities. The photovoltage technique, on the other hand displays recombination centers such as precipitates, dislocation, stacking faults, cracks, and gross damage near a semiconductor surface. Each of these electro-optical imaging techniques provides information about interfaces that was previously inaccessible to observation.

* Work supported in part by the Defence Advance Research Projects Agency and monitored by AFCRL under contract number F 19628-74-C-0077.

Introduction

Focused beams of various types of ionizing radiation have been used in the past[1-20] to probe semiconductor surfaces and devices, generally in the region near a p-n junction. The signal induced in a junction by a scanned optical beam has been found to provide information[3-10] on resistivity fluctuations in the material, on gross defects in the device, and on surface irregularities or inversion layers near the junction. Generally, in this type of measurement, a beam of electrons or photons is scanned across an area of a semiconductor to produce hole-electron pairs in the material. An irregularity in the material will produce a fluctuation in a sample current of some sort detected when the beam scans across the defect. In the standard configuration, a p-n junction collects current produced within a diffusion length of the junction. Any change in either the generation or recombination rate near the junction is detected as a fluctuation of the collected current. The beam induced current is displayed on a rastered CRT to produce an image of the defects and inhomogenities. Imaging techniques of the electron beam induced current[11-20] (EBIC) or photon induced current type[4-10] are useful in identifying defects in individual semiconductor devices, but they cannot easily be applied to the study of semiconductor surfaces or interfaces on which no p-n junction exists. The necessity of using a p-n junction to collect the beam induced current makes non-destructive evaluation of material surfaces at various stages of processing virtually impossible by the beam induced current techniques.

Recently, several scanned beam techniques, including scanned internal photemission[21-24] (SIP), scanned surface photovoltage[25,26] (SSP), and the

corresponding electron beam analogs[27,28] have been developed to probe free semiconductor surfaces. These new techniques provide images of defects near surfaces or interfaces without the necessity of a p-n junction to detect the signal current. As a result, they can be used to examine non-destructively the defects which occur on semiconductors at various stages of material processsing. Each of the techniques has characteristic advantages and capabilities. The e-beam techniques provide the best resolution, better than about 1000 Å,[27] but they are complicated by beam induced charging of any insulating film on the surface.[28] On the other hand, the optical techniques have a resolution capability of on the order of one micron, but they do not charge the surface insulating or passivating film. Hence, the optical techniques can also be used to examine charge non-uniformity in the insulating film on the surface without disturbing the system. Additionally, the optical scanning apparatus can be made to be cleaner than existing e-beam systems because it does not require a complex vacuum system.

Of the optical techniques, SIP determines small inhomogeneities in the contact barrier Φ between two materials, one of which is typically an insulator such as SiO_2. The SIP technique is useful in imaging changes in Φ which are due to contamination, interface chemical reaction, impurity segregation at the interface, or surface crystallographic defects. In contrast, the SSP technique is sensitive to local recombination centers that are within about one micron of the surface and to charge inhomogeneities in the insultating overlayer. Typical recombination centers seen in SSP images include crystallographic defects, precipitates, and gross surface damage; these defects are usually introduced during growth, cutting,

polishing, and high temperature processing of the semiconductor material. The SSP technique has a unique advantage in that no direct contact to the sample is required if the photovoltage measurement is made by capacitive coupling. Since physical contact is unnecessary, the SSP technique is clean and completely non-destructive.

Optical Scanning System

The instrumentation for the two scanned optical techniques is quite similar in that a small spot is rastered on the sample surface while a signal, either photoemission or photovoltage, is detected and displayed on a CRT. A cw laser is used for the light source in order to obtain a measureable signal from a small, nearly diffraction limited light spot. Reasonable signals were obtained with 1.0 mW of light incident on the sample, without any noticeable thermal damage to the sample at the 10^5 W/cm^2 power density at the focused spot. The spot was swept by the sawtooth motion of a galvanometer driven mirror, which was scanned at a 20 Hz rate. In the other direction, the beam was swept slowly in order to complete a 600 line single frame in 30 seconds. The frame rate, which is limited by the rate of the fast scan mirror, could easily be increased an order of magnitude by increasing the fast scan rate to 200 Hz. A further increase, at the expense of a reduced spacial resolution, could be obtained with an accoustic deflection system for the fast scan direction. The total resolution capability of the optical scanning technique is limited by three equally important factors: the divergence of the light output from the laser, the diffraction limit of the objective lens, and the bandwidth of

of the detector. At best, the spacial resolution (of the SIP measurement) is estimated to be about 0.43 microns, with the dominant factors being lens diffraction at $\lambda = 3250$ Å and laser divergence.

The simple optical system shown in Fig. 1 was used to scan a light spot over a square area of the sample surface. Radiation from a laser source was focused onto a 50 micron pinhole in order to eliminate the light that diverged by more than 0.5 mrad. The laser source was chosen to be either an RCA He-Cd laser operating with 3mW at 3250 Å or a Spectra Physics He-Ne laser with 5 mW at 6328 Å. Light emergent from the pinhole was projected a distance of one meter onto a series of two front surface mirrors, which rotate through angles Θ and ϕ. Light from the two scanned mirrors completely filled the aperture of the objective lens for the full range of the scanned angles. Then, the focused spot of light from the objective lens scanned an area of the sample as the two orthogonal mirrors were rotated. The size of the scanned area, and to some extent, the resolution of the system, were determined by the objective lens. The focal length of the lenses used in the measurements range from 0.54 cm to 20 cm. Reflecting objective lenses were used for the high resolution measurements so that correction of the optics for the wavelength of each laser was unnecessary.

The fast scan mirror was driven at about 20 Hz by a rotary galvanometer, G-306, available from General Scanning, Inc. Care was taken to balance the mirror and rotor in order to minimize parasitic oscillation of the mirror assembly. This parasitic oscillation or vibration causes deflection of the light perpendicular to the direction being scanned by that particular mirror. Although faster galvanometer scanners are available, the relatively

conservative rate of 20 Hz was chosen to minimize the problems caused by vibration and to optimize resolution.

The problem of positioning and focusing the sample, something which is particularly difficult in the case of UV light, was solved by detecting light reflected back into the system from the sample. Initially, light from the pinhole goes through the scan system which focuses it onto the sample. When the system is in focus, the light reflected from the sample is focused by the system back onto the pinhole, independent of the mirror positions Θ and ϕ. However, if the system is out of focus, the reflected light falls outside the pinhole where it strikes a flourescent screen. The system is brought into focus by adjusting the sample position along the optical axis until all of the reflected light is refocused back onto the pinhole.

In order to locate the sample in the beam and to examine the surface conditions during the measurements, a reflectivity image of the sample can be obtained and displayed in the coordinate frame of the CRT. A portion of the light reflected from the sample is directed onto a photocell by a beamsplitter. The light falling on the photocell comes to focus at a point which is independent of the same angles Θ and ϕ. Current from the photocell, when displayed as Z-axis modulation of a rastered CRT, forms an image of the sample at the wavelength of the laser source and in the same coordinate frame as the SSP or the SIP image of the same area.

Both the photoemission and the photovoltage signals are detected and displayed on a CRT screen by the circuitry shown schematically in Fig. 2. The signal current is detected by a Kiethley 18000 picoammeter which has

been modified for a fast response; the modification involves a reduction of the feedback capacitance in each of the two amplifier sections, while maintaining the stability of the overall system. The signal in the SIP measurement is the photocurrent, while the signal in the SSP measurement is the capacitive current induced in the probe electrode by the surface photovoltage. The amplitude and dc level of the signal are adjusted and applied to the Z-axis of the CRT, along with a retrace blanking pulse derived from the fast scanner. The X and Y axes of the CRT are driven by voltages proportional to those directly across the drive motor armatures. Images of the Z-axis modulated display of the SSP or the SIP signal are recorded photographically.

The measurement apparatus, shown in Fig. 3, includes the scan mirrors, the galvanometer motors, the reflecting microscope objective, the sample positioning stage, and the picoammeter. Light, incident on the mirrors from the right, is deflected onto the two orthogonally mounted scanning mirrors by a stationary positioning mirror. From the fast scanned mirror, the beam enters the reflecting objective lens (Beck 36/.5) which focusses the light onto the sample. Because of the curvature of the focal plane of this objective, the overall resolution is noticeably degraded for beam deflections greater than ±0.5°. In order to extend the useable field of view, it is necessary to use a refractive plano-objective which is corrected for flatness of field at the laser wavelength.

The sample is held in position and focused by an X-Y-Z adjustable hot stage. Signals from the sample are detected by the picoammeter located behind the hot stage in Fig. 3. The entire assembly is secured to a two

meter optical bench.

Scanned Internal Photoemission

Scanned internal photoemission (SIP) is a relatively recent technique[21-24] for probing interfaces with a beam of light to produce electronically an image or replica of the interface contact barrier. Typical images display a modulation of the internal photocurrent induced by the scanned beam which is due to a lateral inhomogeniety of the contact barrier. The technique is somewhat analogous to scanning electron microscopy (SEM), except that in this case a light beam is used to excite electron emission into a dielectric instead of into vacuum. As in the SEM technique, the emitted current is displayed on the Z-axis of a CRT.

The mechanism of SIP is internal photoemission on a local scale, as shown in Fig. 4. A scanned light beam of energy $\hbar\omega$ penetrates a transparent[29] or semi-transparent[30] electrode and is absorbed in the opposite electrode where it excites electrons into the conduction band. Some of the electrons have sufficient momentum normal to the interface so that they are able to surmount the barrier Φ and reach the opposite electrode. Near threshold, the quantum yield for photoemission is

$$\Psi = \gamma(\hbar\omega - \Phi)^{\alpha},$$

where γ is a constant and α is an empirically determined power, typically in the range 2 to 3. A small percentage reduction in Φ leads to a relatively larger increase in yield,

$$d[\ln \Psi] = \frac{\alpha\Phi}{(\hbar\omega - \Phi)} \quad d[\ln \Phi] .$$

The sensitivity of the SIP technique depends upon the rapid increase of photocurrent produced by a small decrease of Φ below the photon energy $\hbar\omega$. For a reasonable image contrast, the laser and any Schottky barrier reduction are chosen so that $\hbar\omega$ is several tenths of an eV above Φ.

The Si-SiO_2 interface is an interesting candidate for examination by SIP imaging, as can be seen in Figs. 5 and 6. Here, the Si-SiO_2 interfaces have been uniformly coated with about 4×10^{12} Na/cm^2 by electrodeposition in order to reduce the interface barrier[31] from 4.25 eV down to a level that is accessible to the He-Cd laser operating at 3.81 eV. Actually, the sodium acts as a "staining agent," increasing the local photocurrent in those places where ions accumulate on the interface. Since the sodium coverage is influenced by defects, it was found to enhance the SIP contrast around defects. Fig. 5 shows an interesting pattern of dark spots seen in the emission from an Si-Si_2 interface grown on $\sim 10^{20}$ P/cm^3 doped (100) Si. These spots, which are about 10 microns in diameter, have been identified as phosphorous that has segregated onto the Si-SiO_2 interface during high temperature growth[32,33] of the 1000 Å thick SiO_2. Apparently, sodium that does reach the Si-SiO_2 interface is rendered ineffective by chemical combination with the phosphorous lying within a few atomic layers of the interface.[33] These phosphorus islands, observed for the first time by the SIP imaging technique, were found to be correlated with the phosphorous doping density in the silicon substrate. Another type of defect on the Si-SiO_2 interface is seen in Fig. 7 as a line, about 30 microns long, with bright spots at either end. The defect, which lies along the <110> crystallographic direction, is thought to be a stacking fault that has been decorated

by sodium ions. The contrast of the stacking fault is enhanced by the sodium decoration.

The SIP technique was also used to study metal-insulator interfaces such as Nb_2O_5-Bi, which is of interest because of the fast switching found in this structure. The SIP image in Fig. 7 represents photocurrent emitted from a 200 Å Bi electrode into Nb_2O_5. The light source was a He-Ne laser at 1.96 eV, which is close to threshold where the technique is most sensitive. In this system, the contrast mechanism is not simple because of the large number of traps in the Nb_2O_5.

Scanned Surface Photovoltage

Photovoltage images show defects that cause minority carrier recombination on a semiconductor surface. The SSP images have also been found to show any non-uniform charge in the passivating layer on a semiconductor. An SSP image is formed by displaying the first or second derivative of the photovoltage induced by a scanned beam of light on a semiconducting surface. The travelling light spot produces a comet shaped cloud of minority carriers which are captured on the slightly depleted surface, as represented in Fig. 8. Carriers from the moving cloud cover the surface to produce a photovoltage. When the beam passes over a defect, some of the charge cloud is lost to recombination, leading to a dip in the photovoltage. This dip is detected by a capacitively coupled electrode near the surface, and displayed on a CRT. Since the charge cloud is quite large, on the order of the diffusion length, the resolution of images produced directly from the photovoltage is rather poor. The high resolution[25] of the SSP technique is due

to the use of the first or second derivative of the photovoltage to form the image. The differentiation accentuates the signal in the region around the light spot, where the charge cloud density has a logarithmic singularity. In practice, the first derivative is obtained directly by measuring the capacitive current induced by fluctuations of the surface photovoltage.

By using conduction of minority carriers along the slightly depleted surface, it is possible to obtain SSP images at some distance from the electrode. The local photovoltage is coupled to the entire surface by the slightly conducting surface. In some cases, it is necessary to enhance the surface conductivity by generating extra minority carriers by a dc blanket illumination. The resolution of remotely detected images was found to be reduced if the surface conductivity is too low. Also, in order to develop a photovoltage signal, the surface must be depleted, either by a blanket electrode (the electrode can be an aquous solution, as was shown by Lile and Davis[26]), or by a surface treatment such as that produced by dry oxidation of p-type silicon.

The signal S' is proportional to a convolution of the excess local recombination rate R with an experimental sampling function, which is approximately equal to the x-derivative of the charge cloud density n. Mathematically,

$$S'(x_0,y_0) \sim \frac{G\gamma\varepsilon_b\delta}{\varepsilon_\alpha\tau_0 t} \int dxdy \; \frac{dn(x-x_0,y-y_0)}{dx} \; R(x,y) \quad ,$$

where G is the total generation rate, δ is the effective depletion width, ε_b is for the dielectric, and τ_0 if the surface minority carrier lifetime. Ideally, dn/dx would be a singly differentiated Dirac delta function

and the signal S' would then be proportional to dR/dx. Because of the finite size of the light spot, however, the resolution is reduced. In a coordinate system centered on the moving spot, a modified diffusion equation[25] is solved to obtain the charge density n in the region around the scanned spot. The charge density is

$$n = A \exp\left\{-\frac{vx}{2D}\right\} K_0(\kappa r) \quad ,$$

where

$$\kappa = \frac{1}{\sqrt{D\tau_0}} \left\{1 + \frac{v^2\tau_0}{4D}\right\}^{1/2} \quad ,$$

and where K_0 is a modified Bessel function of the second kind and D is the surface diffusion coefficient. The sampling function dn/dx is plotted in Fig. 9 for several scan velocities, with the reasonable parameters D = 15 cm^2/sec and τ_0 = 0.01 sec. The form of dn/dx deviates little from 1/r near the light center at r = 0. Based on this simple theory, the resolution at 1/e is approximately 2.7 times the light spot diameter for singly differentiated SSP and nearly 1.0 for the doubly differentiated technique.

Several examples of SSP images, obtained from (100) silicon surfaces, display the resolution, sensitivity, and comparative advantages of this relatively simple technique. An SSP image of several clusters of emergent dislocations which penetrate the (100) surface of a sample are shown in Fig. 10. The dislocations were produced by mechanically damaging the reverse side of a silicon wafer, and then annealing it in dry He at 800°C for 30 min. It is known that such damage will cause dislocations to propagate through to the front surface during high temperature processing.

Surface defects were also found in SSP images of nominally defect free silicon, an example of which is shown in Fig. 11. Here, a semitransparent blanket electrode was used in order to maximize resolution. The image shows scratches, some as long as 1000 microns, which are not parallel to a low order crystallographic direction. Presumably, these scratches were introduced during the polishing process. Another type of defect, commonly seen in device grade silicon, occurs throughout the area of Fig. 12. These small spots are thought to be crystallographic defects associated with precipitates of oxide or other foreign material. The density of these defects was found to be correlated with oxygen concentration, suggesting that the defect may be associated with an oxide precipitate. The density was found to be as high as $10^5/cm^2$ (within several microns of the surface). A rather uncommmon surface defect, displayed in Fig. 13, was found on a device-grade silicon wafer. It appears to be similar to the surface defects, identified as microsplits by Schwuttke[35], which are small cracks along the <110> direction in the silicon surface with stacking faults at either end. Schwuttke has found that microsplits like that in Fig. 13 are introduced during the saw cutting of the silicon.

It is interesting to compare the SSP technique with the useful but destructive technique of selective etching. A sample was prepared for this purpose by polishing a piece of saw cut silicon at a 2° bevel off normal to the (100) surface. The sample geometry is represented in Fig. 14. A Sirtl etch was applied to half of the surface to reveal the saw damage. The sample was then oxidized and the series of SSP images in Figs. 14 A' - D' were measured. For comparison, Figs. 14 A - D are micrographs of the

etched surface at points of polish depth equal to that of the equivalent SSP image. Both the etch pattern and the non-destructive SSP technique appear to provide the same type of information. However, it is thought that the SSP measurement is sensitive to sub-surface structure such as precipitates which may not appear in an etch pattern.

Conclusion

Each of the scanned optical techniques, scanned internal photoemission and scanned surface photovoltage, has unique capabilities for examining semiconductor surfaces and interfaces. Photoemission imaging is useful in determining interface reaction or contamination. However, it is not amenible to wide use in process control or material evaluation because of the difficulty of the measurement and the requirement of a contacting counterelectrode. On the other hand, photovoltage imaging is a simple, fast, non-contacting, non-destructive technique that offers reasonable resolution, about half a micron for a double differentiated measurement at a wavelength of 3250A. Since scan speed does not degrade resolution, there is no inherent physical limit on the frame repetition rate. The photovoltage technique has been used routinelv to detect stacking faults, dislocations, precipitates, gross surface damage, and local insulator charging.

The photovoltage imaging technique SSP has great potential for use in semiconductor material evaluation and in process control in the production of semiconductor devices. By observing the defects introduced during the various stages of production, it is possible to identify and control the

factors that introduce defects. In the particular case of silicon intergrated circuits, both the production and the reliability of the devices is critically dependent upon crystalline perfection of the material which can be monitored by SSP imaging. The use of photovoltage imaging is somewhat less useful as a research tool than the electron beam analog, as developed by Bottoms[28], because the spacial resolution is considerably lower.

REFERENCES

[1] Adam, G., Physica 20, 1037 (1954).

[2] Avery, D. G., and Gunn, J. B., Proc. Phys. Soc. B 68, 918 (1955).

[3] Oroshnik, J., and Many, A., J. Electrochem. Soc. 106, 360 (1959).

[4] Tihanyi, J., and Pasztor, G., Solid State Electronics 10, 235 (1967).

[5] Potter, C. N., and Sawyer, D. W., Optical Scanning techniques for semiconductor device screening and identification of surface and junction phenomena, Physics of Failure in Electronics, Shilliday, T. S. and Vaccaro, J., Eds., Rome Air Development Center Series in Reliability, 1967, vol. 5, p. 37.

[6] Summers, R. A., Solid State Technology, p. 12, (March, 1967).

[7] Haberer, J. R., Photoresponse Mapping of Semiconductors, in Physics of Failure in Electronics, Shilliday, T. S. and Vaccaro, J., Eds., Rome Air Development Center Series in Reliability, 1967, vol. 5, p. 51.

[8] Phelan, Jr., R. J., and DeMeo, Jr., N. L., Appl. Optics 10, 858 (1971).

[9] Kozhevin, V. E., Sov. Phys.-Solid State 8, 1979 (1967).

[10] Kasprzak, L. A., Rev. Sci. Inst. 46, 17 (1975).

[11] Lander, J. J., Schreiber, H., and Buch, T. M., Appl. Phys. Lett. 3, 206 (1963).

[12] Everhart, T. E., Wells, O. C., and Matta, R. K., J. Electrochem. Soc. 111, 929 (1964).

[13] MacDonald, N. C., and Everhart, T. S., Appl. Phys. Lett. 7, 267 (1965).

[14] Czaja, W., and Patel, J. R., J. Appl. Phys. 36 1476 (1975).

[15] Everhart, T. E., Proc. IEEE 54, 1480 (1966).

[16] Foss, N. A., J. Appl. Phys. 41, 823 (1970).

[17] Ravi, K. V., Varker, C. J., and Volk, C. S., J. Electrochem. Soc. 120, 533 (1973).

[18] Varker, C. J., and Ravi, K. V., J. Appl. Phys. 45, 272 (1974).

[19] Gonzales, J. A., Scanning Electron Microscopy 1974, Johari, O., Ed. p. 94 (ITT Research Institute, Chicago, Illinois, 1974).

[20] T. Kato, T. Matsukawa, H. Koyama, and K. Fujikawa, J. Appl. Phys. 46, 2288 (1975).

[21] T. H. DiStefano, Appl. Phys. Lett. 19, 280 (1971).

[22] T. H. DiStefano, J. Appl. Phys. 44, 527 (1973).

[23] R. Williams and M. H. Woods, J. Appl. Phys. 43, 4142 (1972).

[24] T. H. DiStefano and J. M. Viggiano, IBM J. Res. Dev. 18, 94 (1974).

[25] J. W. Philbrick and T. H. DiStefano, "Scanning Surface Photovoltage Study of Defects in Silicon," in 13th Annual Proceedings, Reliability Physics (las Vegas, Nevada, April 1, 1975) P. 159.

[26] D. L. Lile and N. M. Davis, to be published in Solid State Electronics.

[27] W. R. Bottoms and D. Guterman, J. Vac. Sci. Technol. 11, 965 (1974).

[28] W. R. Bottoms, Daniel Guterman and Peter Roitman, J. Vac. Sciitechnol. 12, 134 (1975).

[29] A. M. Goodman, Phys. Rev. 152, 780 (1966).

[30] R. Williams, "Injection by Internal Photoemission," in Semiconductors and Semimentals, Vol. 6, edited by R. K. Willardson, Academic Press, Inc., New York, 1970.

[31] T. H. DiStefano and J. E. Lewis, J. Vac. Sci. Technol. 11, 1020 (1974).

[32] N. J. Chou, Y. J. can der Meulen, R. Hammer, and J. G. Cahill, Appl. Phys. Lett. 24, 200 (1974).

[33] Y. J. can der Meulen, J. Vac. Sci. Technol. 11, 985 (1974).

[34] D. J. Dumin and W. N. Henry, Metallurgical Trans. 2, 677 (1971).

[35] G. H. Schwuttke, Tech. Rep't. 1,2, ARPA Contract No. DAHC 15-72-C-0274.

[36] The bevel polished sample was prepared by J. W. Philbrick, IBM Hopewell Junction, NY.

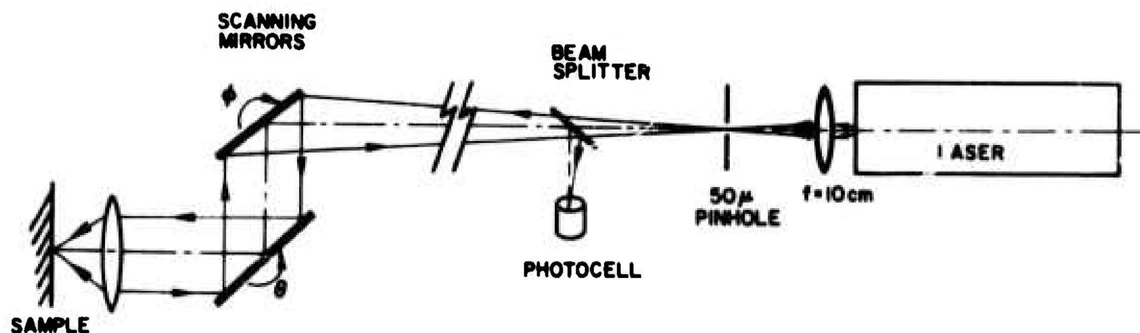

Figure 1 Optical system and measurement apparatus for the scanned optical measurements. Laser radiation is focused through a 50 μm pinhole and then deflected by two scanning mirrors rotating about perpendicular axes. The deflected light fills the aperture of a microscope objective lens for all deflection angles θ and ϕ. The system is brought to focus by adjusting the position of the sample along the optical axis to minimize the size of the light spot reflected onto the fluroescent screen on the back of the 50-μm pinhole. A portion of the reflected beam is diverted and brought to a stationary focus on a photocell in order to detect a reflectivity image of the scanned area.

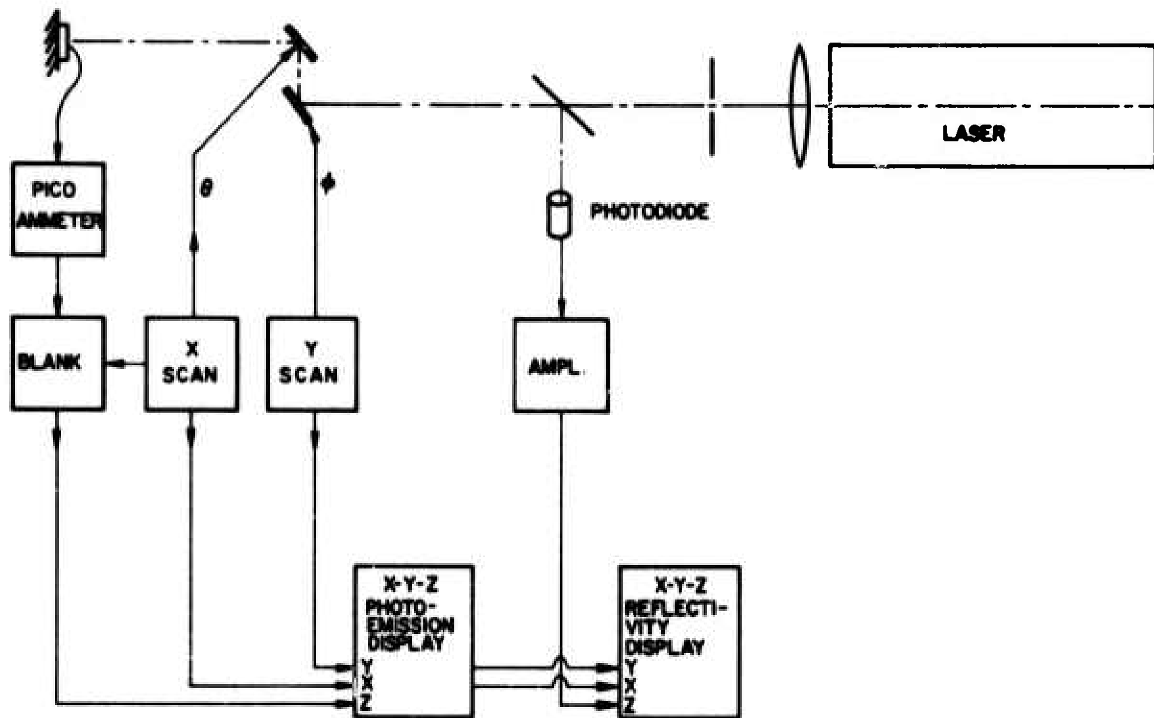

Figure 2 A schematic representation of the scanned optical system showing the instrumentation required to obtain SIP and SSP images. The x and y inputs to the CRT are driven directly by the voltage applied to the mirror galvanometer motors.

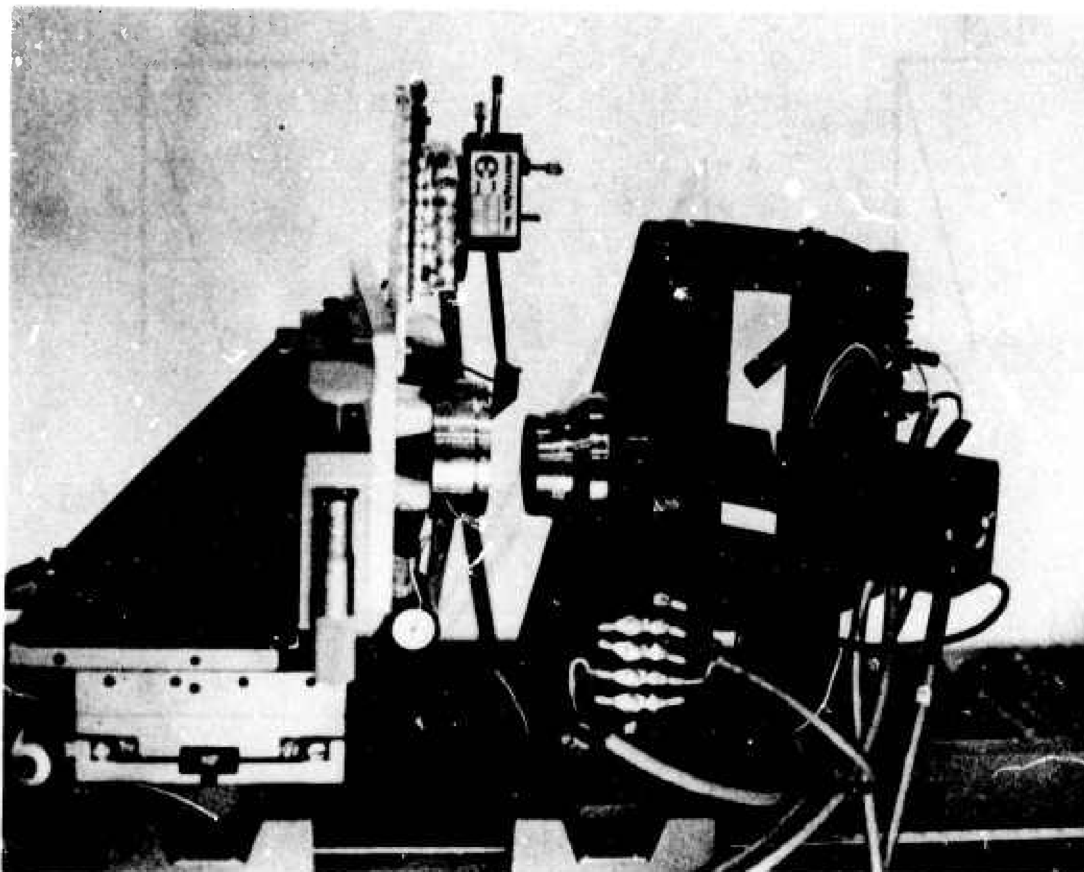

Figure 3 The optical scanning apparatus showing the scan mirrors, galvanometer drivers, microscope reflecting objective, sample positioning stage, and the preamplifier head.

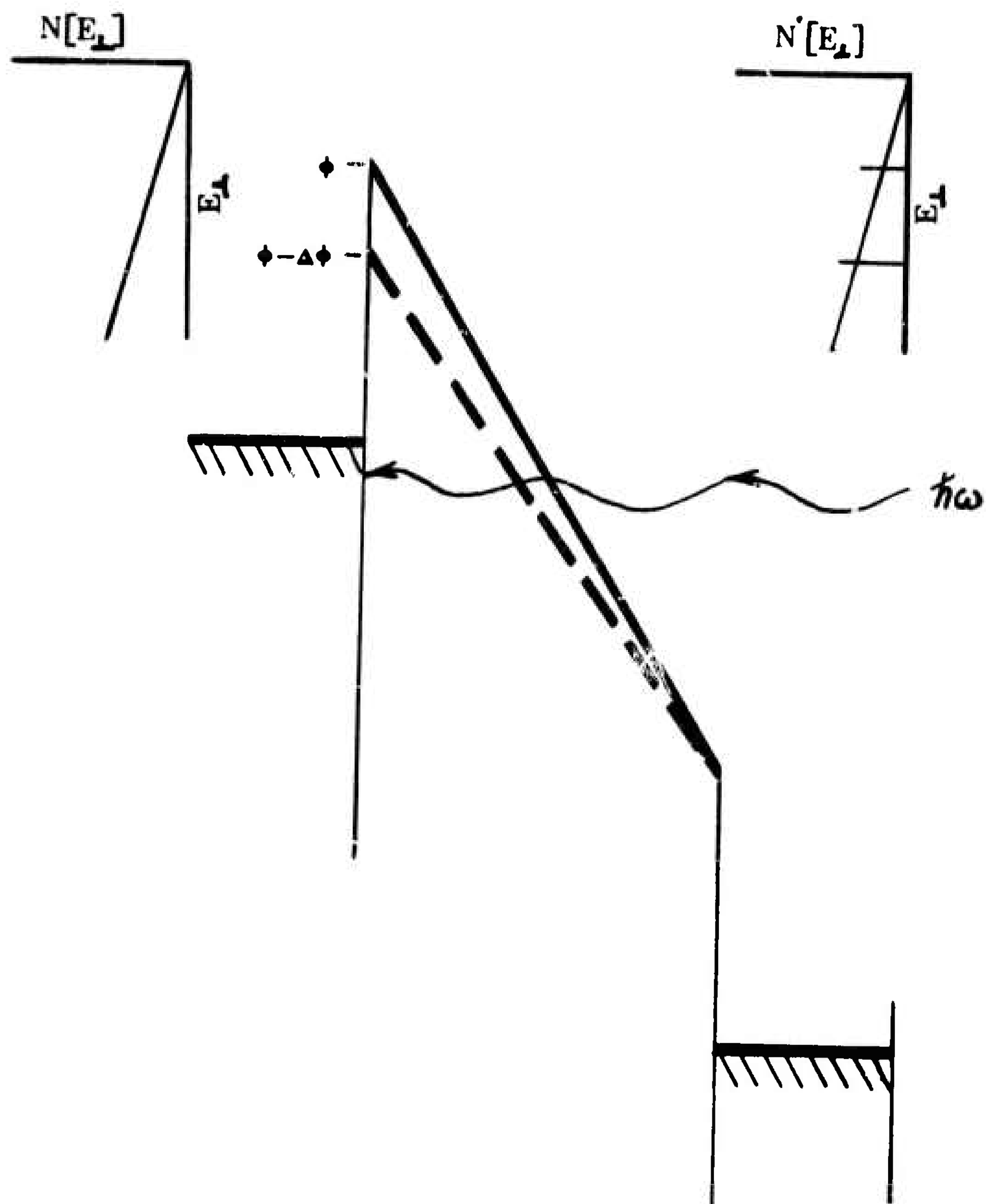

Figure 4 A representation of the processes involved in scanned internal photoemission. A small reduction in the effective interface barrier allows an enhanced photocurrent to flow.

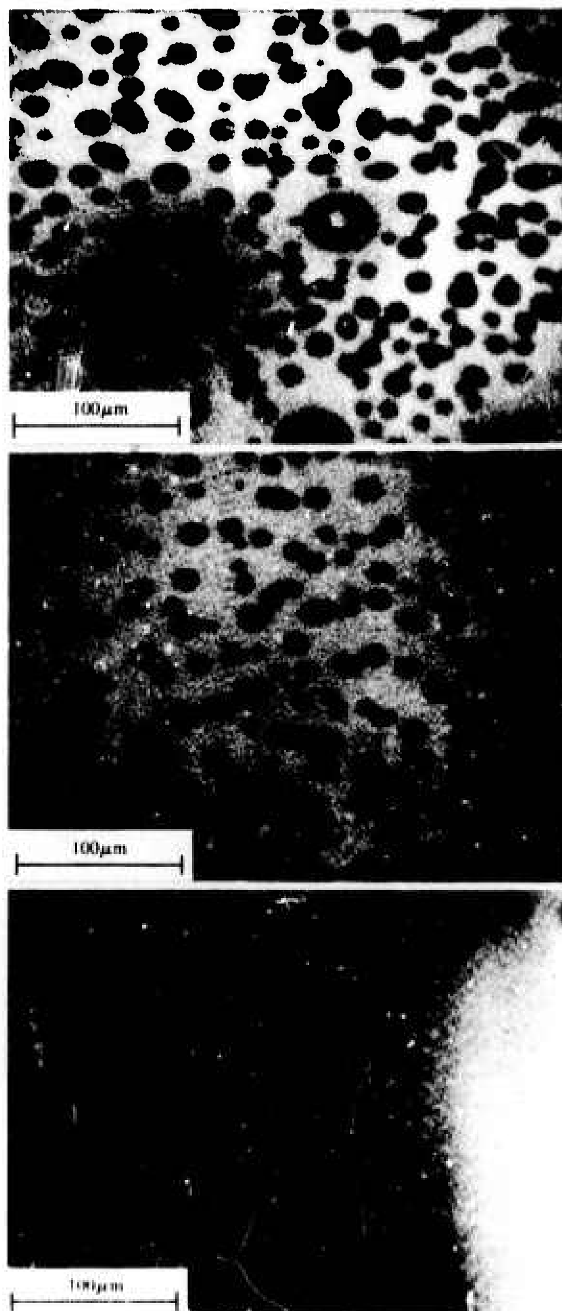

Figure 5 Scanning internal photoemission images of three samples of $Si\text{-}SiO_2$ interfaces covered with $4 \times 10_{12}$ sodium atoms per square centimeter, and measured at a photon energy of 3250 Å. The light areas indicate a high photoyield produced by the presence of sodium on the interface. The dark areas are thought to be due to regions of phosphorus rich layers near the $Si\text{-}SiO_2$ interface. Phosphorus segregates at that interface during the formation of the SiO_2 layer, produced by the oxidation of 10^{20} P/cm^3 doped silicon.

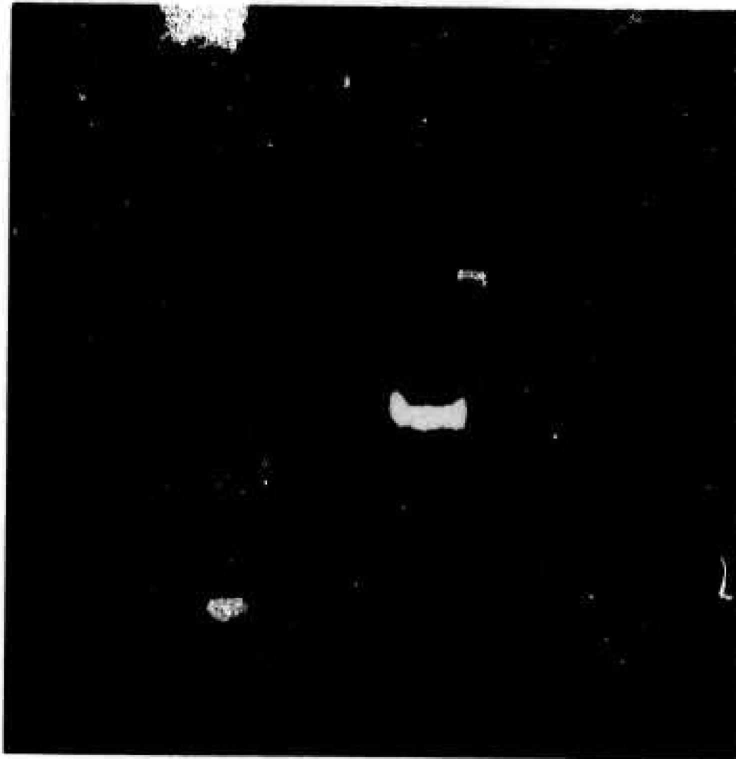

Figure 6   Scanned internal photoemission measurements of an $Si-SiO_2$ interface which has been uniformly coated with 4×10^{12} Na/cm^2. The Na is found to decorate a 30 μm, long defect which lies in the <100> direction on the silicon surface.

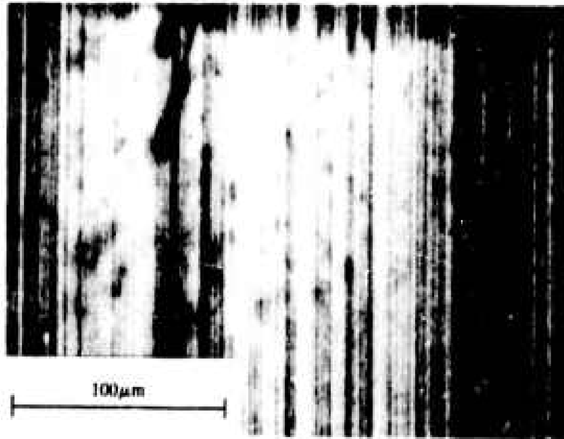

Figure 7 Scanned internal photemission image of a Bi-Nb_2O_5 interface, measure at $\lambda = 6328$ Å. The vertical striae are due to a dc level shift of leakage currents.

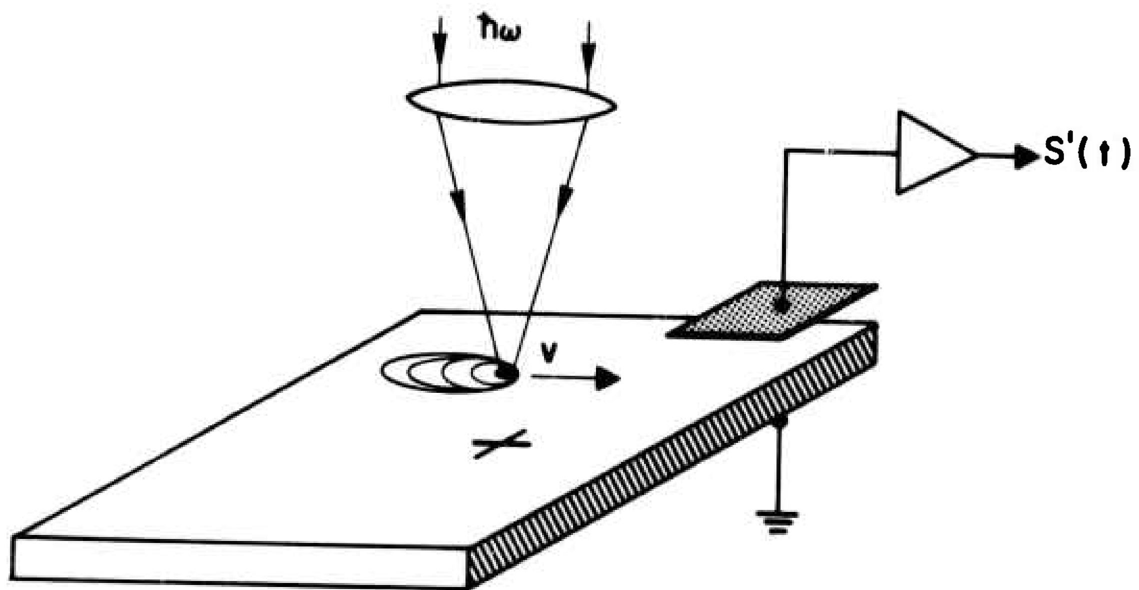

Figure 8 The rudiments of the scanned surface photovoltage measurement. A spot of light is swept across a semiconductor surface, generating a comet shaped cloud of minority carriers in a surface depletion region. The surface potential, capacitively detected by a remote electrode, fluctuates when the spot traverses a surface recombination center.

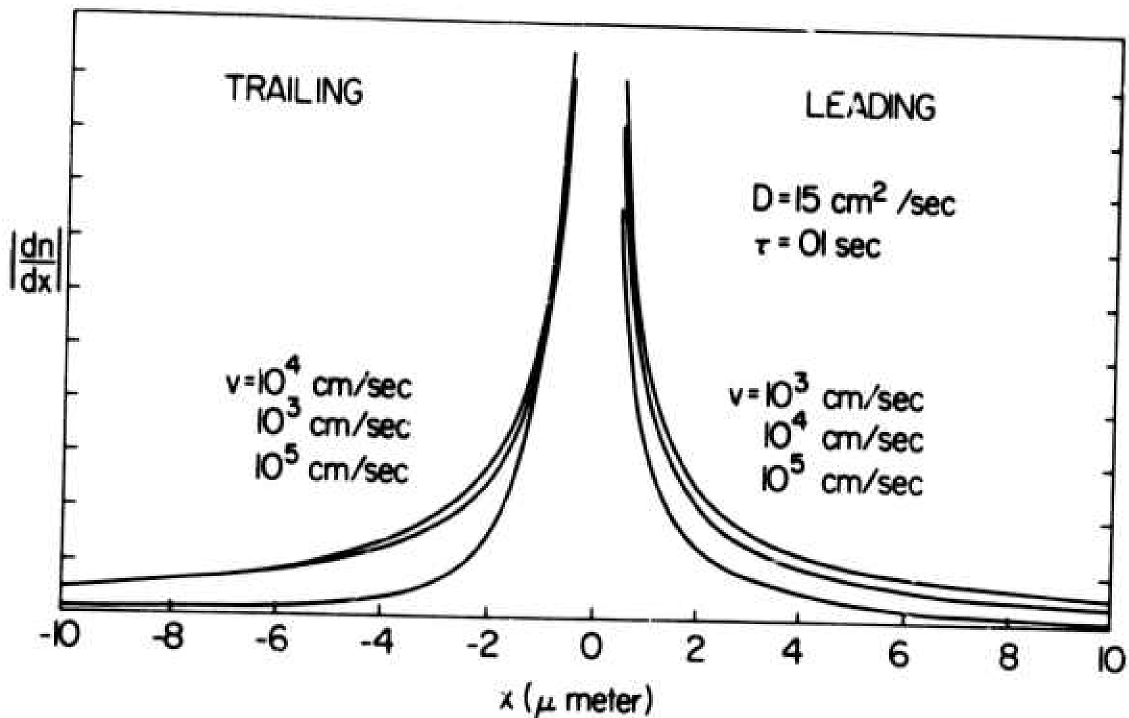

Figure 9 The spacial derivative of the surface minority carrier density, along a line in the direction of travel of a 1μm spot of light. The derivative is relatively insensitive to the scan velocity v for the values shown in the figure. The quantity |dn/dx| is the sampling function in the singly differentiated scanned surface photovoltage measurement.

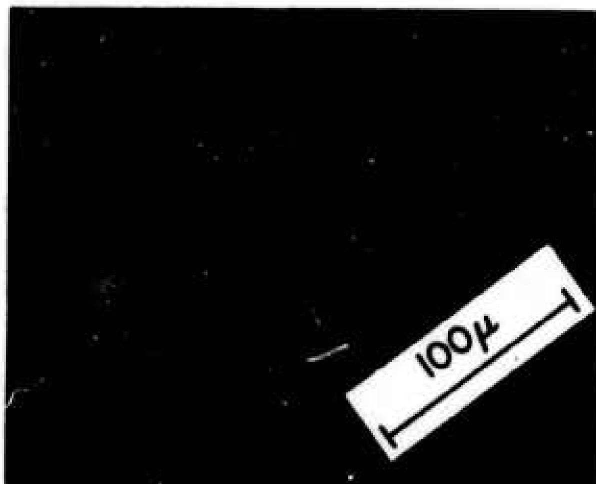

Figure 10 Scanned surface photovoltage image of several clusters of emergent dislocations through the (100) surface of a silicon wafer. The dislocations were generated by sandblasting a spot on the reverse side. During subsequent annealing and oxidation steps, the dislocation loops generated at the damage sites grow through the wafer, eventually penetrating the front surface.

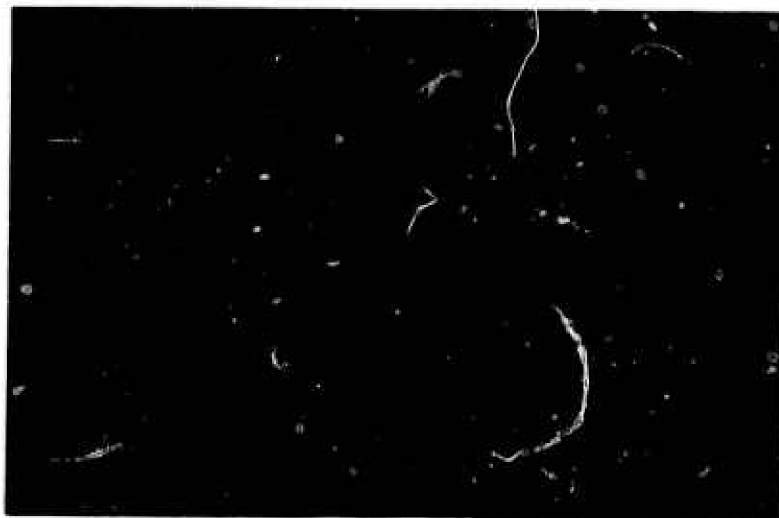

Figure 11 Scanned surface photovoltage image of surface damage produced during the cutting and polishing of a silicon wafer. The damage line does not follow the <100> direction on the (100) surface.

Figure 12 Scanned surface photovoltage image of a (100) silicon surface showing small, randomly distributed defects.

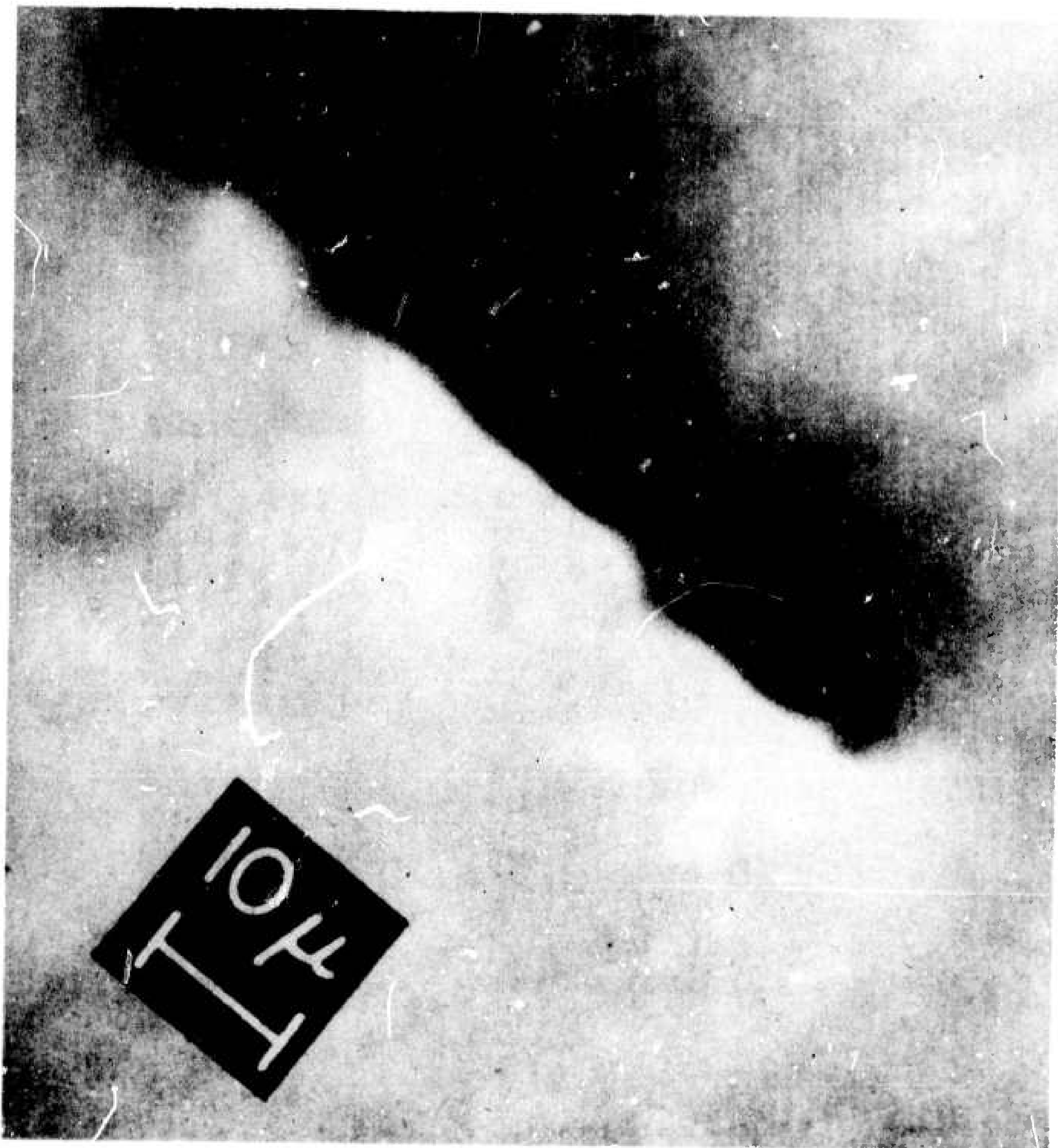

Figure 13 Scanned surface photovoltage image of a defect, apparently a microsplit, which was introduced during saw cutting of the (100) surface. The microsplit is thought to be flanked by stacking fault arrays in the <100> direction on the surface.

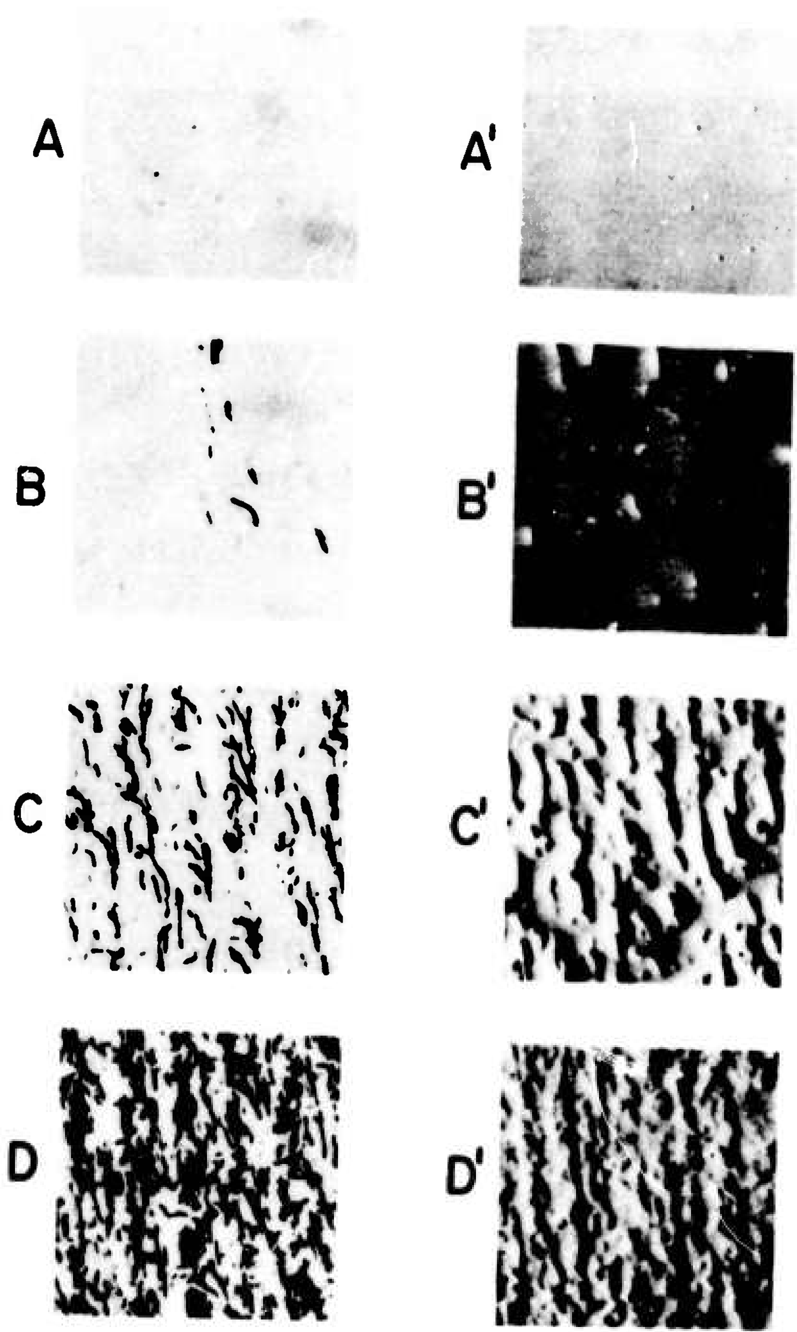

Figure 14 Scanned surface photovoltage images (A', B', C', D',) of saw damage in a silicon wafer which has been polished at a 2° angle. For comparison, micrographs (A, B, C, D,) of an adjacent area of the surface were made after etching. Both sets of images, taken on a highly polished area of the beveled surface, show the transition from the damaged region to the undamaged region occuring at about the same depth, as is observed on an etched portion of the bevel.

IV. FIELD DEPENDENT INTERNAL PHOTOEMISSION PROBE OF THE ELECTRONIC STRUCTURE OF THE $Si-SiO_2$ INTERFACE*

T. H. DiStefano

IBM Thomas J. Watson Research Center

Yorktown Heights, New York 10598

ABSTRACT

Details of the SiO_2 conduction band near the $Si-SiO_2$ interface were examined by the technique of determining the field dependence of the threshold $\Phi(E)$ for internal photoemission for fields up to 7×10^6 V/cm. From a measurement of $\Phi(E)$, the conduction band bottom $\phi(x)$ in the SiO_2 was determined to within approximately two lattice units of the interface. In calculating the effective potential $\phi(x)$, corrections were made for the effects of the photon induced tunneling and field penetration into the silicon. The results of conduction the threshold measurements show only a small deviation from a flat band, approximately +0.05eV, up to a point 4Å from the silicon surface. There is no indication of a large ionic charge or of a greatly reduced SiO_2 bandgap to within about two lattice units of the interface.

* Work supported in part by ARPA and monitored by AFCRL under Contract No. F 19628-74-C-0077.

INTRODUCTION

Although the $Si-SiO_2$ interface has been studied far more intensively than any other because of its technological importance, the details of the electronic and physical structure of the interface are little understood. The lack of information about the region near the $Si-SiO_2$ interface is due to the difficulty of probing only the first few atomic layers around the interface without otherwise disturbing the system. Certainly, one would not expect that the interface between a given crystallographic surface of Si and an amorphous SiO_2 layer is precisely atomically smooth. In fact, it is not unreasonable that the first few molecular layers of SiO_2 and Si might be irregular. Evidence[1] based on He backscattering data suggests that SiO_2 which has been thermally grown on silicon contains excess silicon near the $Si-SiO_2$ interface. Recent He backscattering measurements, which employed atomic channeling to minimize background, show approximately 6×10^{15} $Si-SiO/cm^2$ in excess of stoichiometry near a thermally grown $Si-SiO_2$ interface. However, ion backscattering measurements are somewhat insensitive and difficult to interpret because of the background from the substrate, even if channeling techniques are employed[3].

Several sputter-etch profiling techniques have been used to examine the $Si-SiO_2$ interface, including Auger[4,5] and ESCA[6] measurements. Data from the sputter-etch measurements show some irregularities near the $Si-SiO_2$ interface which have been variously interpreted as excess Si in the SiO_2, a graded bandgap interface $Si-SiO_x-SiO_2$, or as free silicon inclusions in the SiO_2. However, the data are difficult to interpret unequivocally due to non-uniformities in the microscopic sputter-etch rate in SiO_2 which causes the

interface to appear distorted because some portions of the silicon surface and exposed by the sputter-etch process regions before others. Additionally, these profiling techniques are complicated by details of the electron escape mechanism and by the physical damage induced by the sputtering process itself. Thus, the sputter profiling techniques are particularly difficult for the $Si-SiO_2$ interface, in which the physical interface is to extend over a region which is on the same order as the uncertainties in the measurement.

In this paper, we provide new information on the local microscopic structure of the $Si-SiO_2$ interface obtained by the field dependent internal photoemission[7] technique. In this technique, the electric field dependence of the threshold for internal photoemission is measured and used to determine the conduction band energy in the insulator as a function of distance away from the interface. In this way, the SiO_2 conduction band was probed from 4Å to 12Å from the $Si-SiO_2$ interface, and was found to bend only 0.05 eV 0.03 eV, up to a point in the SiO_2 about 4Å from the surface. In view of the 9.0 eV bandgap of SiO_2, the 0.05 eV band bending is small. We see no substantial evidence for an SiO_x graded bandgap, or for significant excess charge extending farther than 4Å from the silicon surface.

FIELD DEPENDENT INTERNAL PHOTOEMISSION

The Si-SiO_2 interface has been extensively studied[8-12] by internal photoemission measurements[13]. The interface barrier is determined by finding the threshold for photoemission over the barrier from spectral photoresponse measurements. Monochromatic light is passed through the SiO_2 to the Si, where photons excite electrons over the Si-SiO_2 interface barrier. The threshold is determined[14] by extrapolating a power law fit to the photoresponse, where the best fit is obtained with a power[11] of 2 or 3. Typically the threshold Φ determined from a third power fit is 0.15-0.2 eV lower than that obtained from a second power fit. Thresholds determined by a third power fit, after correction for Schottky barrier reduction, are 4.35 eV[11] and 4.30 eV[12]. In the present work we find an interface barrier of 4.44 eV by using a parabolic fit to the photoyield.

The Si-SiO_2 interface may not be an ideal, abrupt surface, but rather, it may extend over a finite distance. Several possibilities for the influence of any excess Si on the microscopic local structure of the interface are represented schematically in Fig. 1. The solid lines show the valence and conduction bands in SiO_2 near an ideal, abrupt surface, while dashed line (b) illustrates the bands in a graded bandgap junction and dashed line (a) shows the effect of positive charge in the SiO_2 bands near the interface. For the graded bandgap model, the transition from Si through SiO_x to SiO_2 is the continous, with the bandgap of SiO_2[15] increasing from 1.1 eV to 9.0 eV, as shown by curve (b). The graded bandgap model implies that the conduction band in the SiO_2 deviates below the ideal straight line near the interface. The other possibility, shown as the dashed curve (a), involves a band

curvature due to charged Si near the interface. Either of the two models for the influence of possible excess silicon near the interface implies a large curvature of the SiO_2 conduction band. This curvature can be examined by the field dependent photoemission technique.

From the field dependence of internal photoemission from Si into SiO_2, the variation with distance from the interface of the SiO_2 conduction band was determined. The field dependence of the threshold of photoemission from various materials into SiO_2 has been found[9, 10] approximately to follow the simple Schottky barrier reduction that one would expect from an ideal abrupt junction. However, any curvature of the SiO_2 conduction band near the interface would result in a deviation from this simple Schottky barrier reduction, as is illustrated in Fig. 2.

The experiment consists in illuminating the Si with photons of energy $\hbar\omega$, which excite electrons e^- in the Si. Electrons with sufficient energy can surmount the interface barrier formed by the maximum of the sum of the conduction band potential $\phi(x)$, the image potential $(-e/16\pi\varepsilon\varepsilon_o x)$, and the applied potential $-xE$. As can be seen in the series of curves for fields E_1, E_2, and E_3, an increase in the applied electric field moves the position of the barrier maximum closer to the interface and lowers the total barrier height. An additional effective reduction in the measured photoelectric threshold is introduced by photon assisted tunneling. Electrons with energy nearly sufficient to surmount the interface barrier have a finite probability of tunneling through the effective barrier for high applied electric fields for which the barrier is relatively narrow. The apparent decrease $\Delta\phi$ in the measured threshold, shown in Fig. 3 for the parameters of SiO_2, is relatively

small, even at the highest electric fields used in the present work. The correction for photon-assisted tunneling is included in the results, although the effect introduced a deviation of only 0.025 eV in the resulting determined $\phi(x)$. From a measurement of the photoelectric threshold $\Phi(E)$ as a function of electric field, the conduction band potential $\phi(x)$ can be determined[7]. By this field dependent photoemission technique, the SiO_2 band curvature was measured as a function of distance away from the silicon surface.

The measurements were performed on samples formed by the oxidation of 10 Ω-cm n-type Si (100) in dry O_2 at 1050 C. The thickness of the SiO_2, determined by ellipsometric measurements, was 1090 Å. A semitransparent electrode of 160Å of aluminum, 0.3 cm in diameter, on top of the SiO_2 was used to apply the electric field and to collect the photocurrent. Photoemission measurements were made up to the highest electric field at which the sample was stable. Three independently fabricated samples were measured, with virtually identical results.

The photoemission measurements were performed with light chopped at 6 Hz in order to minimize 1/f noise and a small residual surface photovoltage, as well as to reject the Fowler-Nordheim dark tunnel currents at the higher electric fields. The spectral photoresponse was corrected for the reflectivity of the sample. From a plot of the half-power of the photoyield at a given applied field, the threshold was determined by extrapolation. At the higher electric fields, the photoyield near threshold was complicated by a component due to the photoemission of electrons from the conduction band of the inverted silicon surface. This additional component was similar to the photoemission spectra found by Goodman[16] for emission from the conduction band of heavily n-type silicon.

RESULTS

The photoelectric threshold $\Phi(E)$ for emission from Si into SiO_2 is shown as a function of electric field in Fig. 4. The experimental points were determined from a fit of the spectral photoyield to a parabolic dependence on photon energy. Extrapolated to zero electric field, the threshold indicates an interface barrier of 4.44 eV. A fit of the spectra to a third power dependence on photon energy was found to shift the points for $\Phi(E)$ lower in energy by about 0.15 eV, without changing the apparent electric field dependence of the points. A fit to the second power rather than the third power was chosen because it facilitates a separation of the photoyield due to emission from the Si conduction band from the emission for the valence band. In a fit to the third power of the photon energy, the excess emission from the conduction band introduces some uncertainty in the determination of the threshold. The information on the interface region derived from either the second or third power fit is substantially the same, since the field dependences of $\Phi(E)$ determined by both methods are virtually identical.

The experimental points for $\Phi(E)$ at low field E (or equivalently, large distances of the effective barrier from the interface) fit well to the solid line, which is the simple theoretical Schottky barrier reduction, using the value of $\epsilon = 2.15$ for SiO_2. The dashed line is the Schottky theory including a correction for photon-assisted tunneling. The fit of the Schottky lowering theory to the experimental results for Si-SiO_2 is reasonably good, much closer than that for Pt - SiO_2 or Au - SiO_2[7].

From the electric field dependence of $\Phi(E)$ we determined $\phi(x)$, the potential of the conduction band bottom in the SiO_2, by a procedure outlined

previously[7]. In case of $Si-SiO_2$, few iterations are necessary because the measured $\Phi(E)$ deviates little from the Schottky theory. For very small deviations from the ideal, $\Phi(x)$ is approximately,

$$\phi(x) = \Phi_o + \Delta\Phi(E)$$

where Φ_o is the threshold extrapolated to E = 0 and $\Delta\Phi$ is the difference between the measured threshold $\Phi(E)$ and the theoretical Schottky barrier reduction at the field E. The distance x_o is the position of the maximum of the total effective barrier at the field E. Neglecting the correction for photon-assisted tunneling, this distance x_o is,

$$x_o = \left\{ \frac{e}{16\varepsilon_\infty \varepsilon_o, E} \right\}^{\frac{1}{2}}$$

where $\varepsilon_\infty = 2.15$ is the high frequency dielectric constant of SiO_2. The SiO_2 conduction band potential $\Phi(x)$ determined in this way is shown as a function of distance x from the interface in Fig. 5. The solid curve is the potential found without correcting for photon-assisted tunneling, while the dashed curve includes this correction.

The band bending in SiO_2 near the $Si-SiO_2$ interface, as shown in Fig. 5, is relatively small. At 4Å from the silicon surface, the deviation from the ideal flat band is only 0.05 eV, or only 0.55% of the bandgap of SiO_2. The small distortion of the conduction band in the SiO_2 may be due in part to a small amount of positive charge in the SiO_2. From Fig. 5, an upper bound on the maximum amount of positive charge beyond 4Å is $2.5 \times 10^{+12} e/cm^2$.

SUMMARY

The technique of field dependent internal photoemission has been used to determine the conduction band potential in SiO_2 near the Si-SiO_2 interface. Only a small deviation from an ideal abrupt junction was found. The total band bending up to a point 4Å from the silicon surface is only 0.05 eV, at most with an estimated experimental error of ±0.03 eV.

The lack of any significant bending of the conduction band rules out the possibility that a graded bandgap junction extends beyond 4Å from the silicon. Further, the small observed band bending is in the opposite direction to what one would expect from a graded bandgap type of model. Also, no singificant charge ($<2.5 \times 10^{12} e/cm^2$) exists in the SiO_2 beyond 4Å from from the silicon surface.

REFERENCES

1. J. A. Davies, J. Denhartog, L. Eriksson, and J. W. Mayer, Can. J. Phys. 45, 407 (1967); T. M. Buck and G. H. Wheatley, Surface Sci. 33, 35 (1972); W. F. van der Weg, W. H. Kool, H. E. Rosendaal, and F. W. Saris, Radiat. Eff. 17, 245 (1973).

2. T. W. Sigmon, W. K. Chu, E. Lugujjo, and J. W. Mayer, Appl. Phys. Lett. 24, 105 (1974).

3. W. K. Chu, J. W. Mayer, M. -A. Nicolet, T. M. Buck, G. Amsel, and F. Eisen, Thin Solid Films 17, 1 (1973).

4. E. Irene, Unpublished, IBM Research (1975).

5. J. S. Johannessen, W. E. Spicer, and Y. E. Strausser, (1976).

6. S. I. Raider, R. Flitch, and M. J. Palmer, J. Electrochem. Soc. 122, 413 (1975).

7. C. G. Wang and T. H. DiStefano, Crit. Rev. Sol. State Sci. 5, 327 (1975).

8. R. Williams, Phys. Rev. 140, 569 (1965).

9. A. M. Goodman, Phys. Rev. 144, 588 (1966).

10. C. A. Mead, E. H. Snow, and B. E. Deal, Appl. Phys. Lett. 9, 53 (1966).

11. B. E. Deal, E. H. Snow, and C. A. Mead, J. Phys. Chem. Solids 27, 1873 (1966).

12. R. J. Powell, J. Appl. Phys. 40, 5093 (1969).

13. R. Williams, "Injection by Internal Photoemission", Chapter 2 in Semiconductors and Semimetals, Vol. 6, (Ed. R. K. Williardson, Academic Press, New York, 1970).

14. E. O. Kane, Phys. Rev. 127, 131 (1962).

15. H. R. Philipp, Phvs. Chem. Solids 32, 1935 (1971).

16. A. M. Goodman, Phys. Rev. 152, 785 (1966).

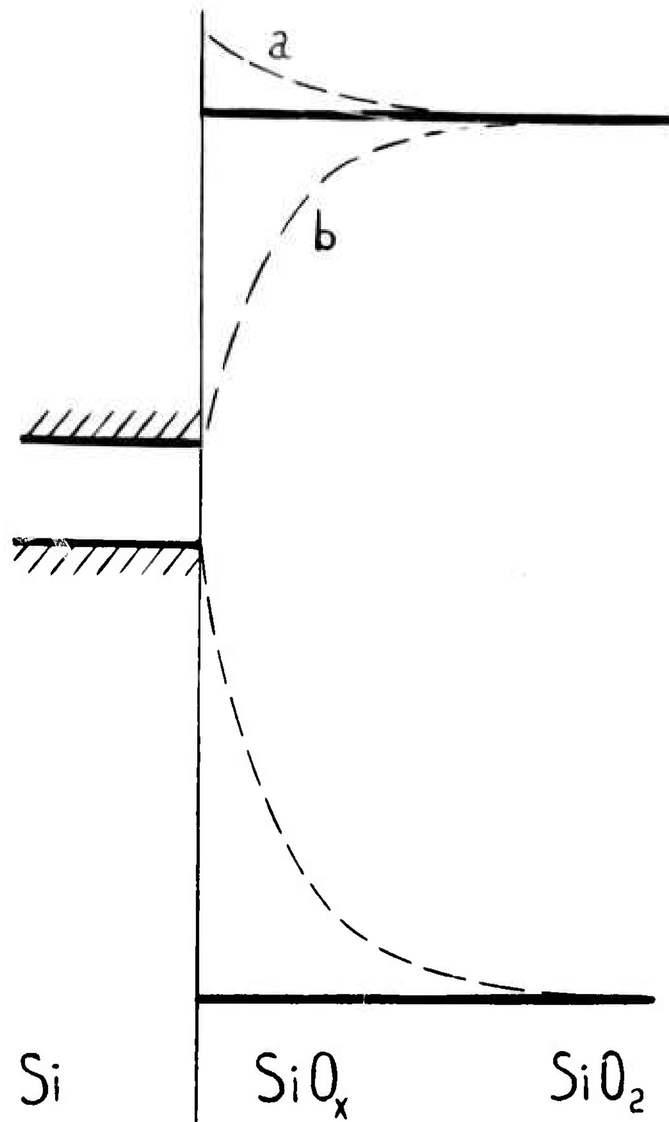

Figure 1 Schematic representation of the electronic bands near the Si-SiO_2 interface. The solid line shows the ideal valence and conduction bands of SiO_2 near the interface, while dashed curves a. and b. represent deviations from the ideal interface due to excess positive charge and a graded bandgap junction, respectively.

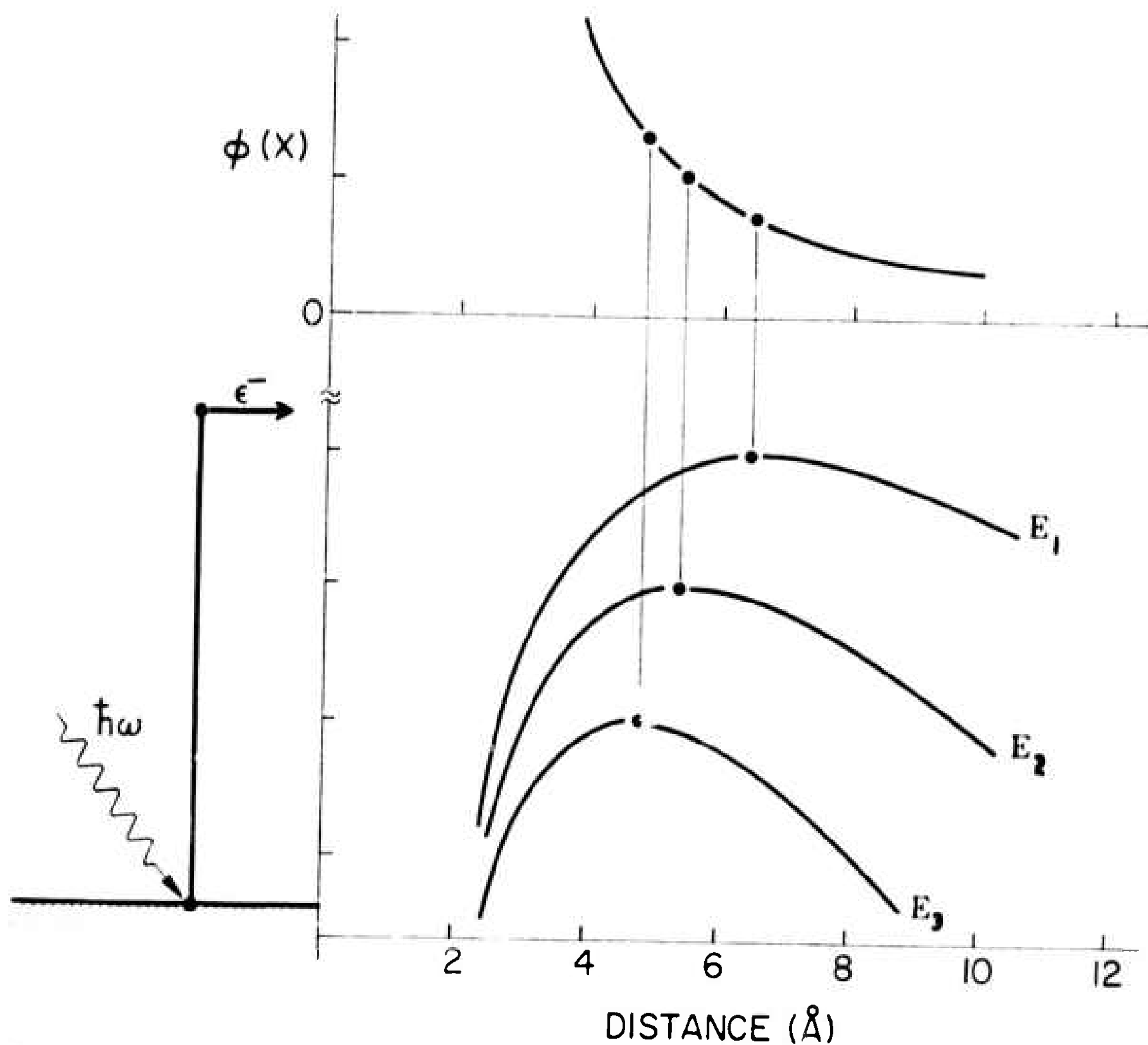

Figure 2 A schematic representation of a Schottky barrier for three different applied electric fields, E_1, E_2, E_3, for the case of an arbitrary initial potential in the insulator. At one particular value of field, the position x_i of the maximum of the barrier and the potential $\phi(x)$ can be obtained from the dependence of the photoemission threshold $\Phi(E)$ upon electric field.

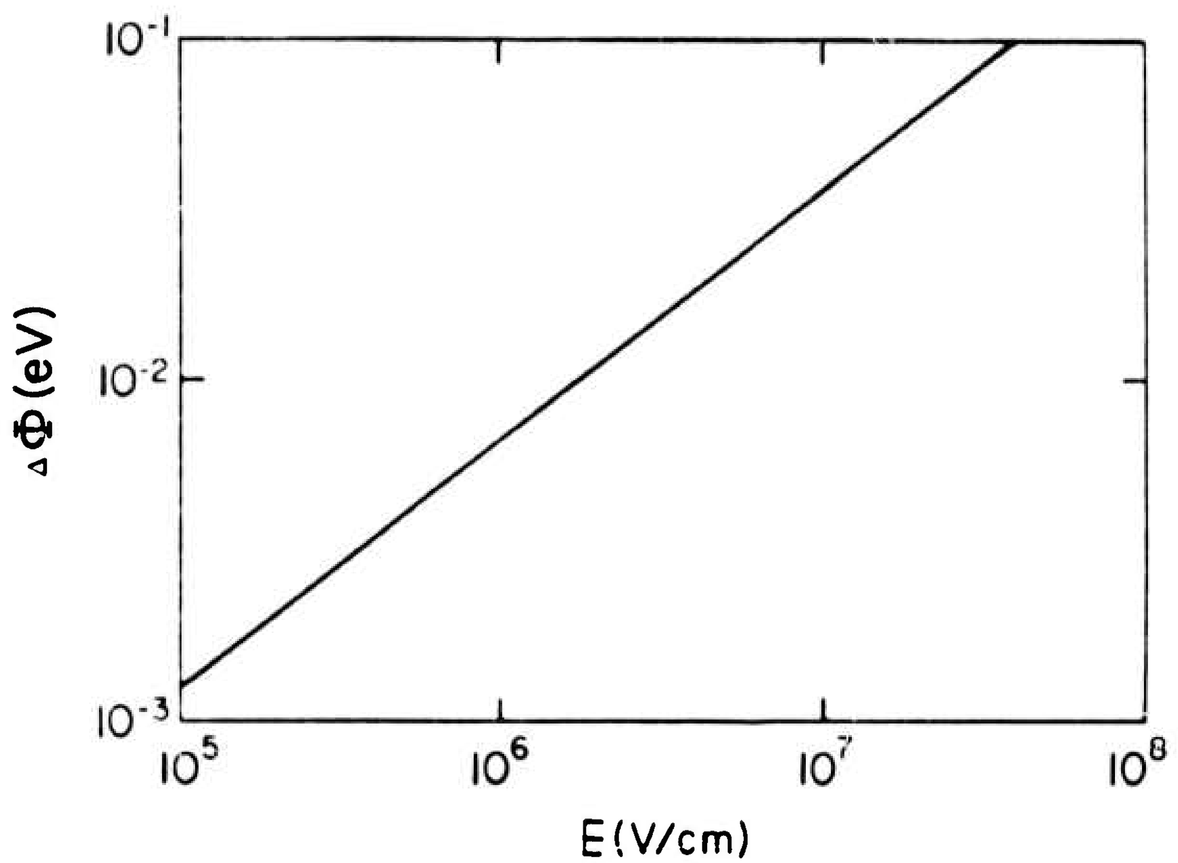

Figure 3 The correction to the photoemission threshold due to photon-assisted tunneling of electrons through the interface barrier. The tunneling parameters are for SiO_2.

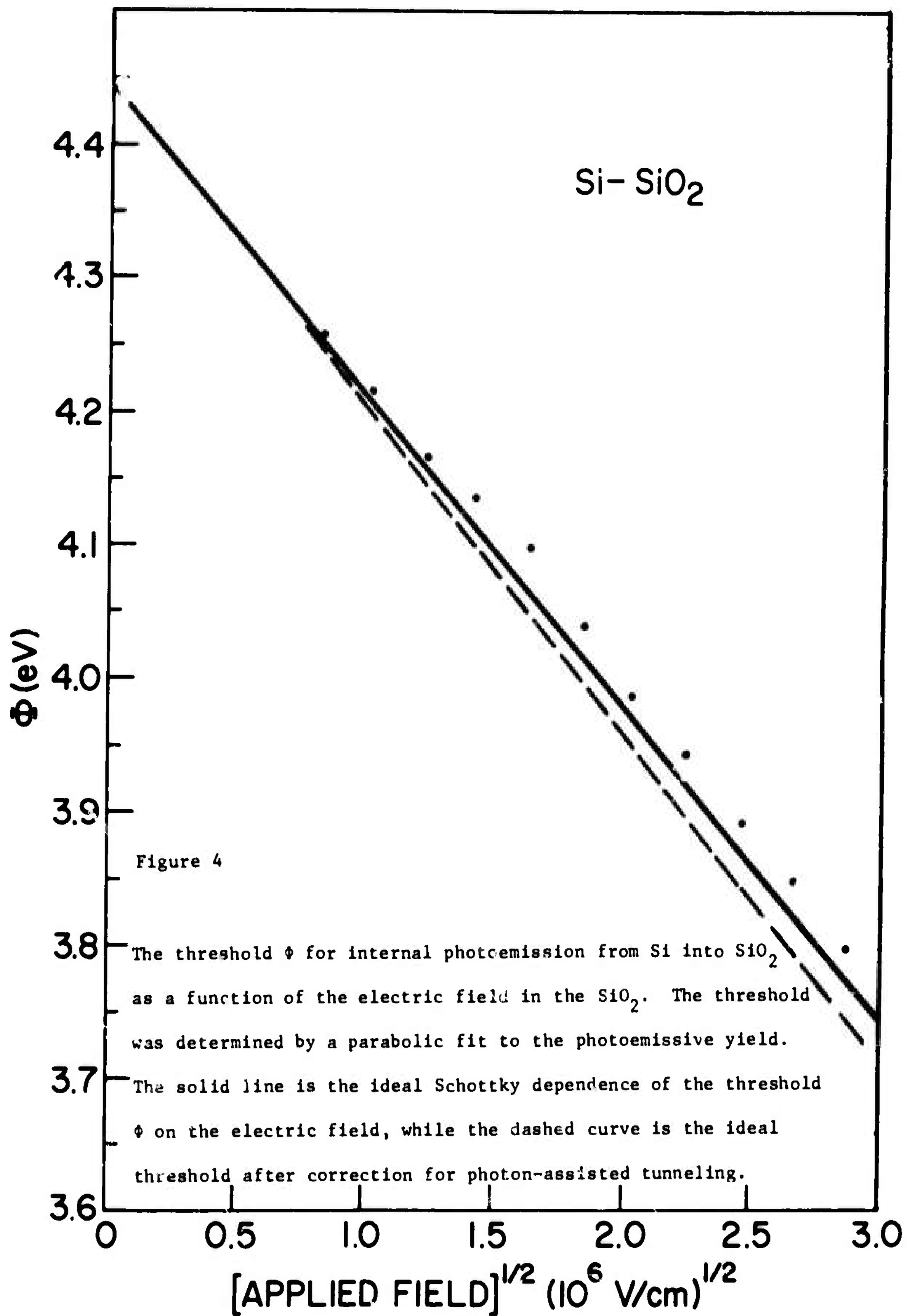

Figure 4

The threshold Φ for internal photoemission from Si into SiO_2 as a function of the electric field in the SiO_2. The threshold was determined by a parabolic fit to the photoemissive yield. The solid line is the ideal Schottky dependence of the threshold Φ on the electric field, while the dashed curve is the ideal threshold after correction for photon-assisted tunneling.

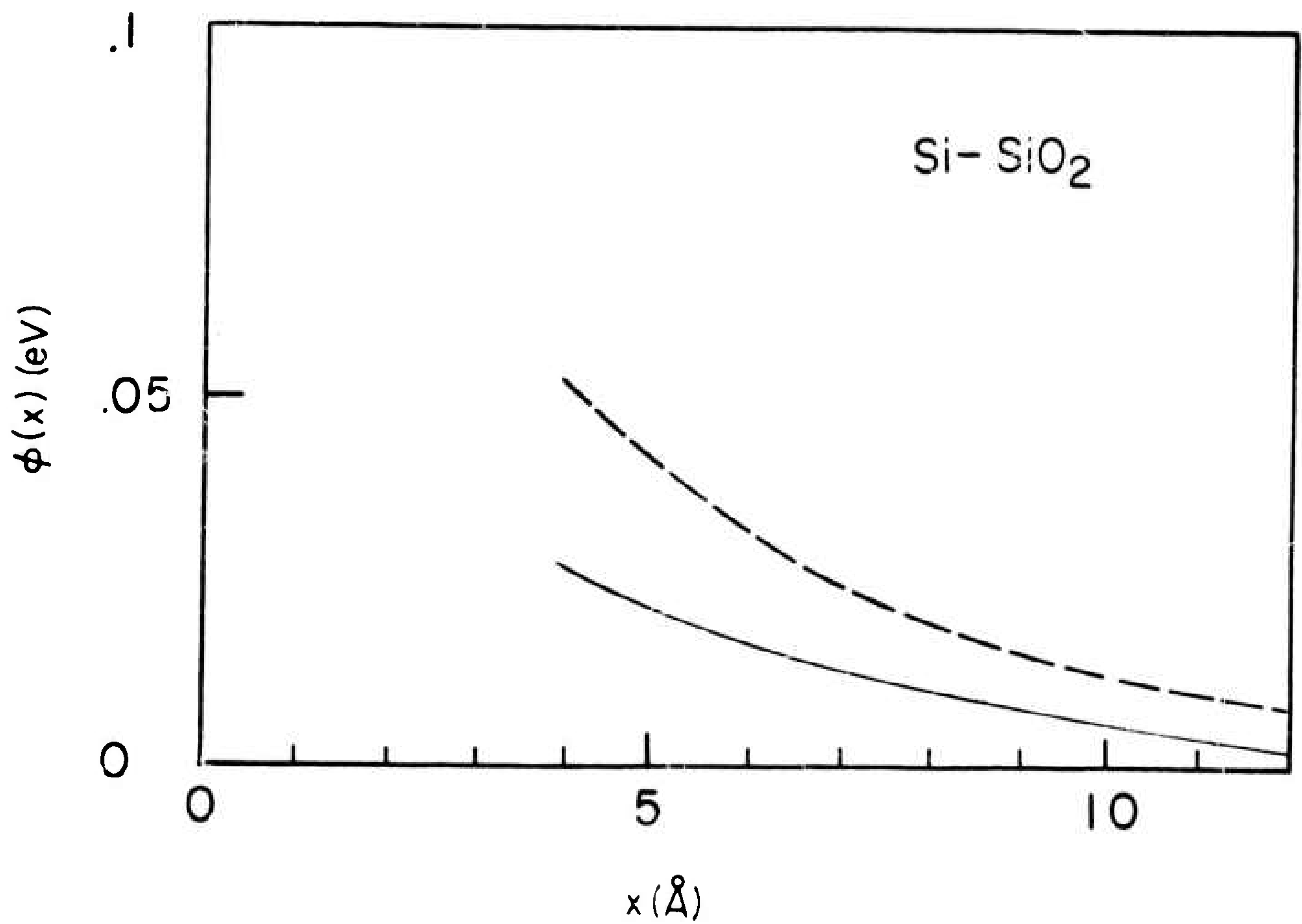

Figure 5 The potential $\phi(x)$ at the bottom of the conduction band in SiO_2 as a function of distance x from the Si - SiO_2 interface. The solid curve is the band bending calculated without the photon-assisted tunneling correction, and the dashed curve is that calculated by including the correction.

V. INTERFACIAL REACTIONS IN SOLIDS

This program is devoted to the study of reaction at metal/silicon and metal/glass interfaces. These two kinds of interfaces are essential elements in MOS devices where the basic structure is multilayered thin films. Multilayered thin films resemble diffusion couples, hence diffusion and interface reaction have been recognized as the prime cause of many reliability problems. Due to the small film thickness, the reaction study demands experimental tools that are capable of detecting structural and compositional variation in a distance of the order of 100Å. Reaction kinetics within such a small distance often is distinctly different from its counterpart in a bulk sample. We have combined a glancing angle Seeman-Bohlin x-ray diffractometer and a MeV $^4He^+$ ion backscattering technique to analyze interfacial reactions. The diffractometer is sensitive enough to obtain the structural information from a metallic film of thickness of 200Å, and the backscattering is capable of profiling the composition variation in a film with a depth resolution of 200Å. These two techniques have been used to measure the growth kinetics of silicide formation. In addition, we have applied implanted noble gas atoms as diffusion markers to determine the dominant diffusing species during the formation.

We now recognize that contract reaction between Si and near-noble transition metals can occur at a much lower temperature than that between Si and other transition metals. The latter requires a reaction temperature above 500°C yet the former can proceed below 200°C. The large discrepancy in reaction temperature indicates atomic mobilities in these two kinds of metal/Si interfaces are different. The silicide tends to

be metal-rich in the low temperature reaction, and to be Si-rich in the high temperature reaction. The use of silicide as a barrier layer on Si has resulted in a wide range of study on properties of silicides, in particular, its formation and growth kinetics. One aspect of silicide formation which has been studied in detial in this program is the identity of the diffusing species.

In conventional bulk couples the faster of the two diffusing species is identified by the direction of displacement of embedded wire markers. To apply this concept to thin film systems requires markers much smaller in dimension than the film thickness. This can be achieved by ion implanting rare gas species which have a depth distribution smaller than the film thickness. Backscattering techniques with MeV $^4He^+$ ions can be used to detect the marker species and their location in depth within the sample.

Implanted noble gas atoms of Ar and Xe have been used as diffusion markers in growth studies of six silicies, Ni_2Si, Mg_2Si, FeSe, VSi_2, $TiSi_2$, and Pd_2Si, formed by reacting metal films with silicon substrates. MeV ^4He ion backscattering has been used to determine the displacement of the markers. The displacement relative to the surface determines the identity of the diffusing species. We found that Si atoms predominate the diffusion in VSi_2, $TiSi_2$ and FeSi, while Ni atoms are the moving species in Ni_2Si and Mg in Mg_2Si. In Pd_2Si both Pd and Si are diffusing species with Si faster of the two. Details of kinetics of silicide formation has been reported in the previous semi-annual reports.

A strong connection exists between silicide formation and glass/metal

reaction. Many metals are known to show detrimental effects on glass; phase separation, devitrification and decomposition. When a metal decomposes SiO_2, it may form oxide and silicide. From the point of view of metal/glass reaction, a metal can be classified as whether or not it forms oxides and/or silicide based on the following reaction equation:

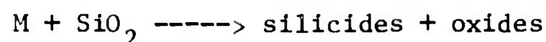

$$M + SiO_2 \longrightarrow \text{silicides} + \text{oxides}$$

where M represents a metallic element. In Table I, we show the four kinds of reactions that can be expected.

Table I: Glass-Metal Reaction

Metallic Elements	Products of the Reactions	
(example)	Silicide	Oxide
Au, Ag	-	-
Al, Sn	-	x
Pt, Pd	x	-
Cr, V	x	x

We have used the Table as a guide for our study and have investigated and reported the reaction with metals in the first group (e.g. Au) and the 4th group (e.g. V). We note that even though Au itself does not react with SiO_2, its eutectic alloy with Si wets and reacts with SiO_2. A case in which such reaction has been found is the MOS structure of $Au/SiO_2/Si$. A wetting experiment with a Au-Si eutectic melt on surfaces of fused quartz has been carried out in He atmosphere. The wetting shows that the melt reacts with quartz. Kinetics of the reaction was studied by annealing an MOS structure of $Au/SiO_2/Si$ at 200 to 800°C in a dynamic vacuum of 2×10^{-6} Torr. Details of the study is reported in the following section.

So far, glass-metal reactions have been found to show detrimental

effects on the integrity of glass. Thus, it is desirable to strengthen glass to show a better resistance to attack by metailic atoms. Structurally, the network configuration of a glass is very loose and could be packed into a denser form. A denser form of glass is ideally better whenever a very thin glass layer (< 1000Å) is required because thin glasses are especially vulnerable to pin holes. We have developed a new technique which potentially may be applied to densify a glass layer and to reduce its pin hole density. The technique is to expose the glass to a low dosage, high energy ion beam. The amount of compaction has been measured by Talystep and confirmed by the changes of density and reflective index obtained by ellipsometry. The densified glass layer has also been found to show an improved dielectric breakdown strength. Details of the study is reported here.

VI. SURFACE REACTIONS ON MOS STRUCTURES

by

K. N. Tu, D. R. Campbell, E. I. Alessandrini and S. Libertini

IBM Thomas J. Watson Research Center
Yorktown Heights, New York 10598

ABSTRACT: A wetting experiment with a Au-Si eutectic melt on surfaces of fused and single crystal quartz was carried out in an atmosphere of He. The wetting showed that the melt reacted with quartz and the wetting angle was about 10 degrees. Kinetics of the reaction was studied by annealing an MOS structure of $Au/SiO_2/Si$ at 700 to 800°C in a dynamic vacuum of $2x10^{-6}$ Torr. In the initial stages, reduction rate of the oxide layer by Au-Si eutectic followed an approximately linear dependence on time and its temperature dependence was characterized by an activation energy of about 26 kcal/mole. The reduction ceased when depletion of Au took place.

INTRODUCTION

We have reported a low temperature surface reaction in MOS structures which results in the degradation of the oxide layer.[1] The MOS structure was made by depositing arrays of dots of Au film on 800Å thick thermal oxide layers on Si wafers. When this structure was annealed at temperatures ranging from 500 to 800°C in a dynamic vacuum of 2×10^{-6} Torr, the Au was observed to diffuse through the oxide and to form a liquid Au-Si eutectic with the underlying Si. The eutectic dissolved the oxide and then spread laterally from edges of the Au dots along the SiO_2/Si interface into areas that were not covered by the Au. A detailed description of the morphology and reaction products has been given,[1] and the most significant finding was that in the reacted areas there was no oxygen, indicating the destruction of SiO_2. We have proposed that the destruction of SiO_2 is due to its reaction with liquid Au-Si eutectic, since no such reactions have been observed with pure Au on fused quartz or on bare Si wafers.[1]

If our explanation is correct, it would suggest that the liquid Au-Si eutectic wets a SiO_2 surface, otherwise there is no reaction between the two. This paper is a study of the wetting of Au-Si eutectic on fused and single crystal quartz surfaces. The results show that the eutectic does indeed react with quartz surfaces. A preliminary study of the kinetics of the eutectic-glass reaction was performed using the Au/SiO_2/Si structure, and the rate and activation energy were given in a earlier report.[2] These and additional kinetic results will now be analyzed further to give a more detailed picture of the reaction mechanisms.

EXPERIMENTAL

(a). Wetting of Au-Si Eutectic on Fused and Single Crystal Quartz Surfaces

A eutectic Au-Si alloy was made by mixing pellets of Au of six-9 purity and pieces of Si from a Si wafer, and annealing the mixture in a sealed quartz tube at 500°C for 24 hours. The mixture had a composition of 69 at % Au and 31 at % Si, in agreement with the eutectic composition in Hansen's book.[3] The alloy was broken into pieces for subsequent wetting experiments and each piece weighed about several grams. The wetting experiments were carried out on a hot stage maintained at 450°C in a titanium-gettered, He atmosphere. A sketch of the hot stage is shown in Fig. 1. The temperature was measured by means of a thermocouple inserted in the Al block which held the quartz wafer. The fused quartz substrates were 1" diameter wafers 1/16" thick. The single crystal quartz had the C-axis normal to its surface and had dimensions of 1"x1"x $\frac{1}{16}$ ".

To determine the wetting angle, we spread the liquid alloy in the form of a stripe on quartz surfaces, kept them at 450°C for 15 minutes to allow local equilibrium to be reached at the edges and then solidified the stripe. The angle was measured on the cross-section of the stripe by cutting across it.

(b). Reaction Kinetics in Au/SiO_2/Si Structure

The layered structure was made by depositing arrays of circular dots of Au film 30 mil in diameter and 500Å in thickness on 80 mil centers onto Si wafers oxidized with 800Å of SiO_2. An optical micrograph of the top view of a Au film dot reacted at 700°C for 4 hours is shown in Fig. 2a. The oxide under and in the vicinity of the Au film was consumed, forming

the circular opening, due to the eutectic-oxide reaction. In Fig. 2b, a scanning electron micrograph of a circular opening is shown. The channels in the opening are parallel to [110] directions of the Si substrate. At the end of each channel where it meets the edge of the oxide we have found a bead of Au-Si. A replica electron micrograph of the channels, the beads, and the interface between the reacted and unreacted areas is shown in Fig. 2c. We have measured the migration rate of the interface between the reacted and unreacted areas, and the spacing between channels as a function of time and temperature. The measurement of the rate was not straightforward since the reaction often does not proceed uniformly over the entire circumference of an Au dot. We chose to measure its average rate over a wide reaction front. To determine its time dependence, we have followed the reaction at a specific area over a selected sequence of annealing times. The spacing between the central line of two channels was determined by averaging measurements over 10 to 20 spacings.

RESULTS AND DISCUSSION

When we broke the sealed quartz tube to take out the Au-Si eutectic, part of the eutectic alloy was found to stick to the wall of the tube. The tube fractured as it was forced apart from the eutectic and pieces of the fractured quartz still adhered to the eutectic. This is a clear indication that the eutectic has wetted the quartz surface.

When the eutectic pieces were placed on the hot stage, they melted at roughly 390°C, which indicates that the pieces were richer in Si than the alloy at the eutectic point. At first, no wetting on the fused quartz surface could be detected, this was probably due to the presence of a surface oxide coating on the melt which existed before the metling and had prevented

the melt from making direct contact with the quartz. When we broke the coating with a pointed Au wire, the shiny, silver-colored liquid wetted the quartz and stuck to the quartz surface wherever we spread it. It also maintained its shiny surface at 450°C throughout the experiment (~ 30 minutes).

The wetting angle as measured from cross-sections of eutectic stripes is about 10 degress. In Fig. 3 an optical micrograph of such a cross-section is shown. Since there is a volume shrinkage at solidification, the measured angle may differ slightly from the true wetting angle. The measurement on the quartz crystal was performed in the same manner and the wetting angle is about the same. There is also a wetting between the bead and the oxide in Fig. 2. However, the wetting angle is not well defined since the oxide was thin and the underlying Si might have altered the angle.

To investigate the eutectic-oxide reaction kinetics, an MOS structure of $Au/SiO_2/Si$ was used instead of samples of Au-Si eutectic on quartz. This is because the progressive enlargement of the oxide-free circular opening is easily monitored from optical micrographs such as the one shown in Fig. 2a. Taking radial measurements of the circular opening at selected intervals of time allows one to plot growth curves as shown in Fig. 4. The basic features of these curves are the linearly rising portion at early times and the leveling-off at long times. The leveling-off can logically be attributed to the depletion of Au.

Before we analyze these reaction curves, the driving force of the reaction should be discussed. It is most likely the lowering of free energy of liquid Au-Si alloy by dissolving oxygen. In the dynamic vacuum condition,

if we assume that the Au rich alloy can release oxygen to the vacuum rather quickly, the alloy is always below its solubility limit and therefore, under a driving force to dissolve more SiO_2. In dissolving the oxide, the alloy gains some silicon in addition to oxygen. We believe, however, the solution of Si to the alloy is not the driving force since the alloy can obtain sufficient Si from the underlying substrate. It appears that the pumping out of oxygen must also be accompanied by the pumping out of some of the Si. This is because each of the channels as shown in Fig. 2c is, on average, 5 microns in width and 0.4 microns in depth; the Si that was in the channel has disappeared. Presumably the partial vapor pressure of Si of liquid Au-Si alloy at 700 to 800°C is high enough so Si can be pumped out easily. The morphology of the channel with a bead of Au-Si at its end appears similar to the reverse process of vapor-liquid-solid (VLS) mechanism of crystal growth of Si whiskers.[5,6] In our case, the reason that the bead stays at the interface rather than drills a hole into the Si substrate as in the VLS case might be its wetting adhesion to the oxide.

In analyzing the reaction kinetics, two pieces of information seemed significant. We know from the wetting experiments that there is an interfacial reaction between the eutectic and the oxide and from the leveling-off of reaction rates at longer times we know that the supply of Au to the reaction interface is crucial. These suggest that the kinetics might be controlled by one or a combination of the following steps; the interfacial reaction, the diffusion of Au to the reaction interface, and the diffusion of Au along the reaction interface. We have assumed here that the formation of the eutectic alloy at the reaction temperatures is so fast that it is kinetically irrelevent.

Also, the time needed for penetrating the oxide layer under the Au dot is treated as an incubation time of the lateral reaction. The constant reaction rates show clearly that at the early stage they do not depend on diffusion of Au from the circumference of the dot to the reaction interface, rather they may depend either on interfacial reaction or on diffusion of Au along the reaction interface as both can give rise to a constant reaction rate. In the latter case, its morphology is similar to cellular reaction, e.g. precipitation or dissolution of Sn from Pb-rich Pb-Sn alloys.[7] In such reactions, the rate takes the following form,

$$\frac{dr}{dt} \cong \frac{D_b \delta}{S^2} \tag{1}$$

where D_b is the diffusion coefficient along the reaction interface, δ is the effective interface width and S is the interlamellar spacing. Assuming this is the rate controlling step, we can estimate the term $D_b \delta$ in the present case. Values of measured $\frac{dr}{dt}$ and S in the temperature range of 700 to 800°C together with the estimated $D_b \delta$ are listed in Table I.

In the Table, there are two features that are worth considering. First, the spacing seems to be independent of temperature in the temperature range measured. This is not what one would expect in a diffusion controlled reaction. Secondly, the effective interface width is hard to guess but is conceivably larger than 5Å, the value accepted for most abrupt solid-solid interfaces. This is because the interface considered here is between solid SiO_2 and liquid Au-Si alloy, so the flux of Au will not be limited in the interface but rather throughout an extended region in the liquid. This is supported by microprobe scanning x-ray micrographs which have shown the presence of Au along and behind the interface. Then if we

take δ to be much wider than 5Å, we find D_b to be much smaller than 10^{-5} cm^2/sec, the value which is accepted as a lower bound for diffusion in liquid metals and alloys. So we conclude that the observed reaction was not controlled by diffusion along the interface.

We have, in the above, eliminated the possibilities of rate controlling by diffusion to and along the reaction interface, so the remaining one that may control the rate is the interfacial reaction, the dissolution of SiO_2 by the eutectic. Assuming there is always an ample supply of Au-Si eutectic at the edge of the oxide, the volume rate of dissolution of oxide will depend on the area of oxide exposed to the eutectic. That is,

$$\frac{dV}{dt} = 2\pi rh\ K(T,P(O_2)). \qquad (2)$$

Where V is the volume of oxide film consumed, r is the radius of an assumed circular opening, h is the oxide thickness and $K(T,P(O_2))$ is the reaction rate constant which will depend on temperature and the partial pressure of O_2. The above expression may be reduced to

$$\frac{dr}{dt} = K\ (T,P(O_2))\ . \qquad (3)$$

This result indicates that an initial loss of oxide should occur at a constant rate for any given T and $P(O_2)$. Since there was no provision in our temperature controlled vacuum furnace for measuring O_2 partial pressure, we assumed that a constant total gas pressure was indicative of a steady state condition in which the pressures of ambient gases such as O_2 remained sensibly constant. Therefore, the slope of the linearly rising portion of the growth curve was employed to determined dr/dt. Furthermore, the slope of a plot of ln dr/dt vs 1/T (Fig. 5) yielded an activa-

tion energy in the customary manner for Arrhenius plots. Proceeding in this manner the activation energy for oxide reduction under a dynamic vacuum of 2×10^{-6} Torr was approximately 26 kcal/mole.

This result is necessarily very approximate as any detailed model would certainly have to include the diffusion of Au through SiO_2 and to the reaction interface. We mentioned that the diffusion of Au through SiO_2 and the destruction of the oxide under the Au have been treated here as steps included in the incubation period of the reaction. Since our experimental approach was geared to observing the lateral reactions, it was not possible to draw any direct inference about the vertical or through-the-thickness reaction of Au on SiO_2. However, calculated values of diffusivity using the data of Badaiov and Shuman[8] are sufficiently large, 7×10^{-16} and 4×10^{-14} cm^2/sec at 700 and 800°C, respectively, to account for several hundred Å penetration of Au during typical incubation times of $\sim 10^3 - 10^4$ sec. Ordinary diffusion processes do not seem adequate to explain the extensive chemical changes which must accompany or precede the destruction of the underlying oxide. Perhaps the Au penetration process is more complex involving a Au-SiO_2 reaction analogous to what Madams, Morgan and Howes[9] reported in their backscattering study of Au migration through SiO films. Clearly, the nature of the diffusion process is not well understood and could warrant further study. It can be stated, however, that the energy we measure is considerably less than the dissociation energy of SiO_2 by thermal energy alone (~ 9eV) and demonstrates the efficiency of the Au-Si eutectic melt for oxide reduction.

Finally, at longer reaction times, the longer diffusion distance might become the rate limiting factor and should affect the constant

reaction rate. But more critical at the end of the reaction is the depletion of Au at the edge of the oxide. This is due to the initial finite amount of Au which has to be distributed to an increasingly bigger area and the loss of Au to the substrate. As the depletion takes place, the rate will decrease and eventually the reaction stops.

CONCLUSIONS

(a) A eutectic melt of Au-Si has been found to wet surfaces of fused and single crystal quartz. The wetting shows that the eutectic reacts with quartz and the wetting angle is about 10 degrees. The eutectic, after solidification, was found to bond rather strongly to quartz surfaces.

(b) An MOS structure of Au/SiO_2/Si has been used to study the kinetics of reaction between Au-Si eutectic and thermally grown SiO_2 at temperatures between 700 to 800°C in a dynamic vacuum of 2×10^{-6} Torr. The reaction proceeds at a constant rate with an activation energy of 26 kcal/mole. The reaction will slow down and stop if depletion of Au occurs.

Acknowledgements

The authors are grateful to K. Asai, W. Kateley and J. Kucza for sample preparation, J. Kuptsis for the SEM picture, C. Aliota for the replica micrograph, and J. C. McGroddy for helpful comments.

References

1. E. I. Alessandrini, D. R. Campbell and K. N. Tu, J. of Appl. Phys. 45, 4888 (1974).

2. E. I. Alessandrini, D. R. Campbell, K. N. Tu, J. Vac. Sci. Technol. 13, 55 (1976).

3. M. Hansen, "Constitution of Binary Alloys," McGraw-Hill, New York (1958).

4. Private communication with Prof. D. Turnbull and Dr. C. C. Tsuei.

5. R. S. Wagner and W. C. Ellis, Appl. Phys. Letters 4, 89 (1964).

6. R. S. Wagner, W. C. Ellis, K. A. Jackson and S. M. Arnold, J. of Appl. Phys. 35, 2993 (1964).

7. K. N. Tu, Metal. Trans. 3, 2769 (1972).

8. A. Z. Badalov and V. B. Shuman, Fizika i Tekhnika Poluprovodnikov, 2, 741 (1968). [Sov. Phys. Semiconductors, 2, 615 (1968)].

9. J. C. Madams, D. V. Morgan, M. J. Howes, J. of Appl. Phys. 45, 5088 (1974).

Table I

Measurements of Reaction Rate and Spacing

Temp. °C	Reaction rate, $\frac{dr}{dt}$ cm/sec	Spacing, cm	$D_b\delta$ cm^3/sec
700	7.8×10^{-6}	1×10^{-3}	7.8×10^{-12}
750	16.2×10^{-6}	1×10^{-3}	16.2×10^{-12}
800	22.2×10^{-6}	1×10^{-3}	22.2×10^{-12}

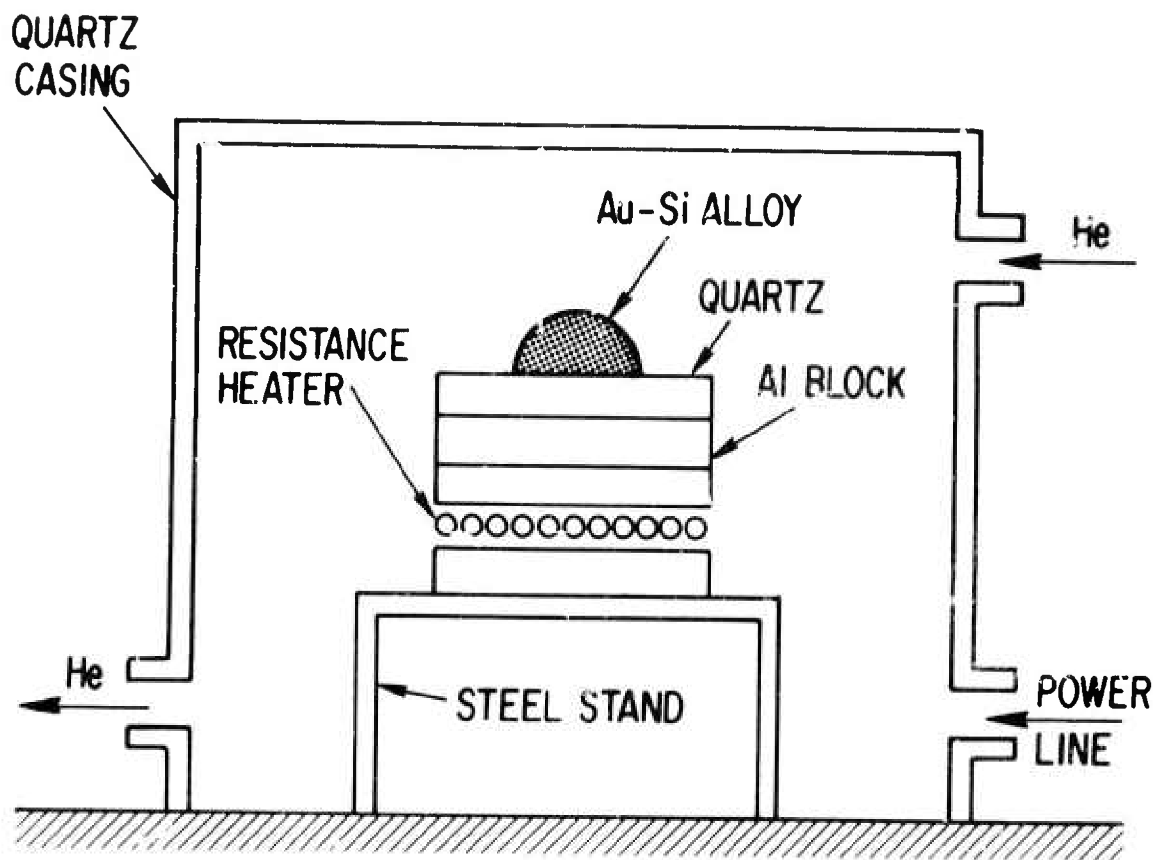

Fig. 1. A sketch of the hot stage used for wetting measurement.

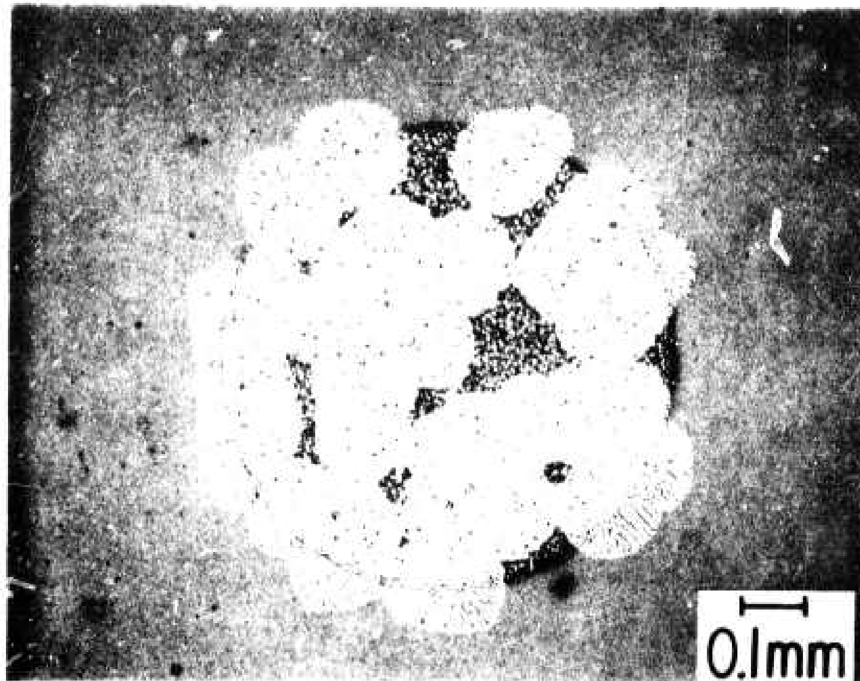

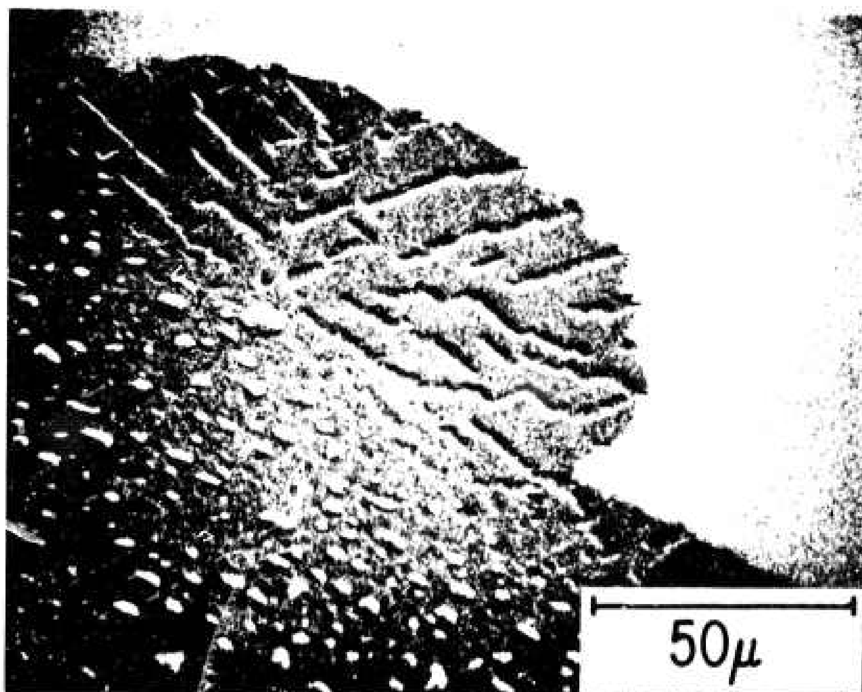

Fig. 2. (a) Optical micrograph of a $Au/SiO_2/Si$ structure after reaction at 700°C for 4 hours. The circular opens are areas where reaction has taken place and no oxygen can be detected.

(b) Scanning electron micrograph showing the channels of a circular open. The channels have been found to be parallel to [110] directions of the Si substrate.

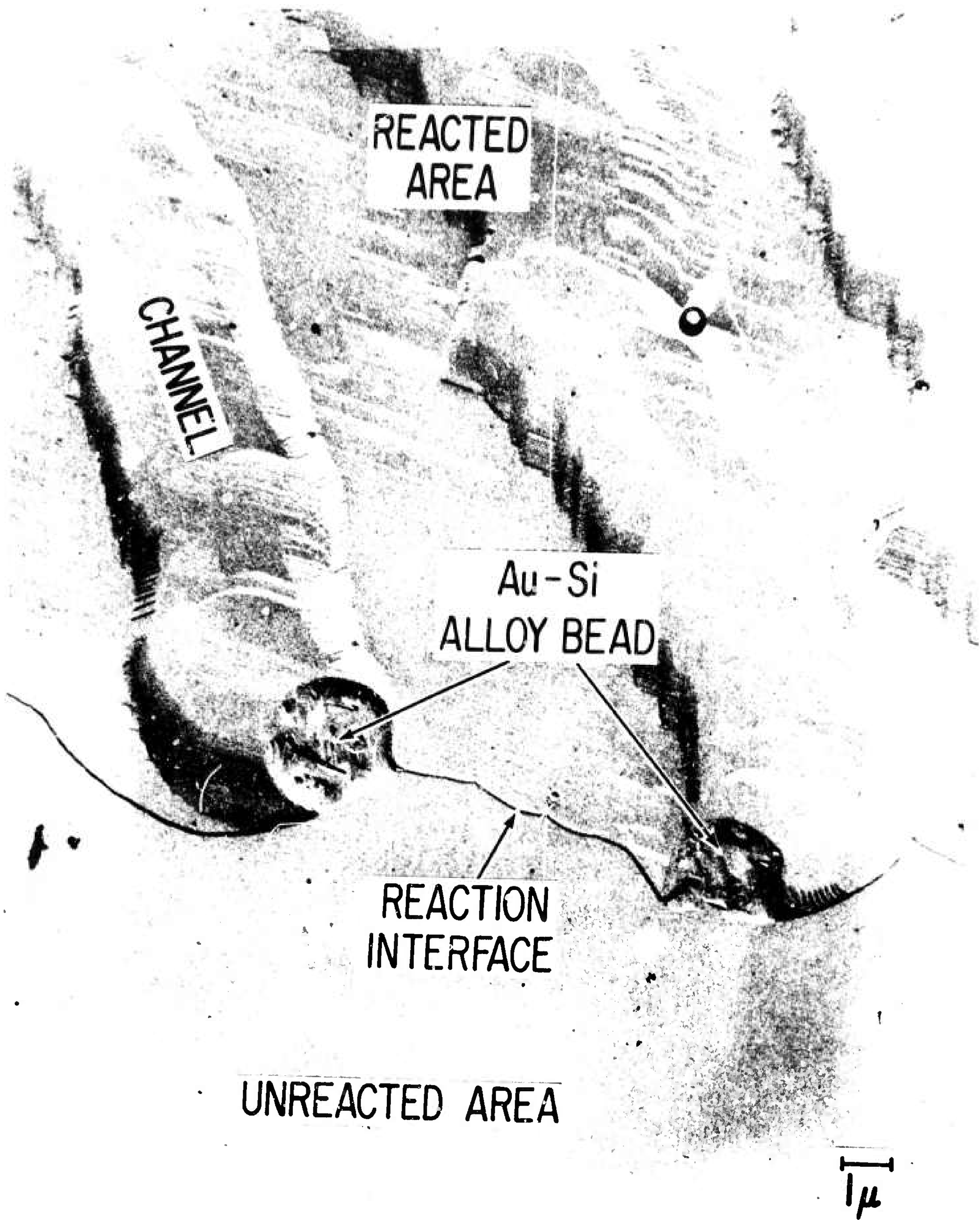

(c) Replica electron micrograph of a reaction front showing the channels, Au-Si eutectic beads and the interface. The sphere with a white shadow is a latex ball of 0.5 microns in diameter.

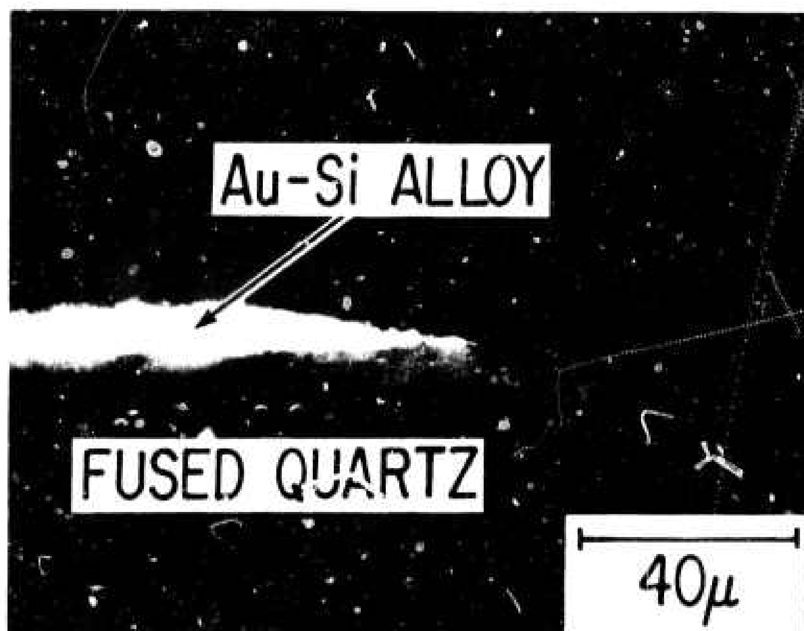

Fig. 3. A wetting edge of Au-Si alloy (near eutectic composition) on fused quartz surface. The angle was measured after the solidification of the Au-Si stripe.

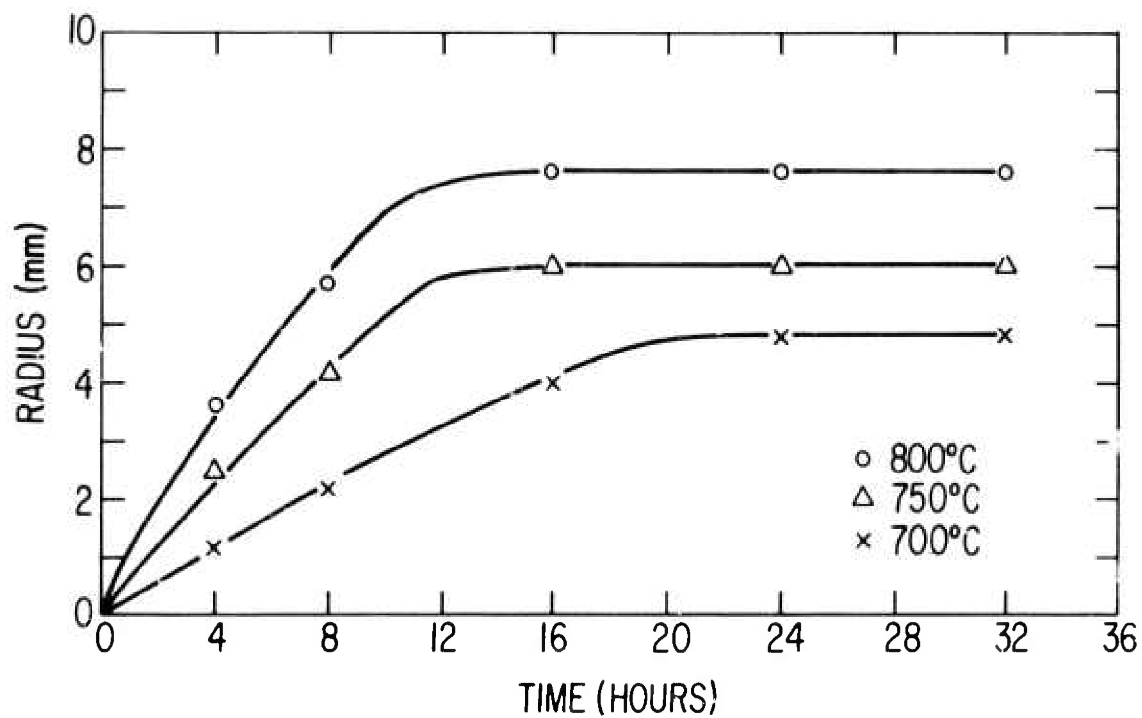

Fig. 4. Reaction rate of liquid Au-Si eutectic with thermally-grown SiO_2 using MOS structure of $Al/SiO_2/Si$ annealed at 700, 750 and 800°C in a dynamic vacuum of $2x10^{-6}$ Torr. The thickness of Au and SiO_2 were 500Å and 800Å, respectively.

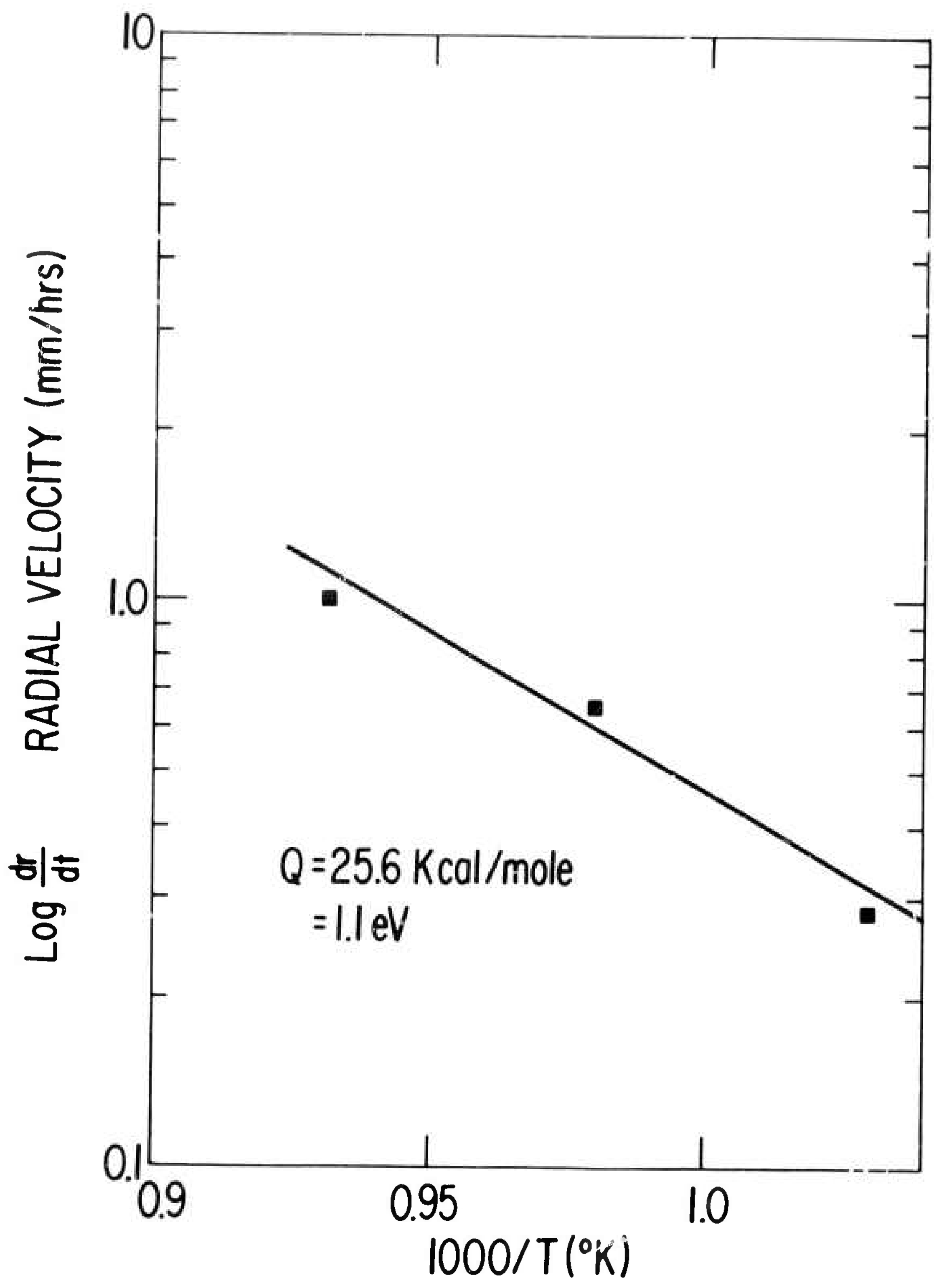

Fig. 5. Plot of log $\frac{dr}{dt}$ vs $\frac{1}{T}$ for the reaction of liquid Au-Si eutectic with thermally-grown SiO_2.

VII. Publications under F19628-73-C-0006 and F19628-74-C-0077

1. T. H. DiStefano "Dielectric Breakdown Induced by Sodium in MOS Structures," JAP 44, 527 (1973).

2. E. I. Alessandrini and D. R. Campbell, "Catalyzed Crystallization and Transformation in SiO_2 Thin Films," Journal of Electrochemical Society. 121, 1115 (1975).

3. D. E. Eastman, "Quasi-Elastic Electron Scattering in EuO; A Possible Explanation for Observed "Paramagnetic" Spin Polarized Photoemission," Physical Review, B8, 6027 (1973)

4. R. B. Laibowitz, S. Herd and P. Chaudhari, "Structural Transformations as Observed by TEM during Electrical Switching in Amorphous Ge-Te," Philosophical Magazine. 28, 1155 (1973).

5. D. R. Campbell, E. I. Alessandrini, K. N. Tu and J. E. Lewis, "Phosphorus Diffusion in Partially Crystallized Films of SiO_2," J. of Electrochemical Society, 121, 1081 (1974).

6. K. N. Tu, J. R. Ziegler and C. J. Kircher, "Formation of Vanadium Silicides by the Interaction of V with Bare and Oxidized Si Wafers," Applied Phys. Letters, 23, 493 (1973).

7. T. H. DiStefano and J. M. Viggiano, "Interface Imaging by Scanning Internal Photoemission," IBM Journal of Research and Development. 18, 94 (1974).

8. T. H. DiStefano and J. E. Lewis, "Influence of Sodium on the Si-SiO_2 Interface," J. Vac. Sci. Technol. 11, 1020 (1974).

9. J. W. Mayer and K. N. Tu, "Analysis of Thin Film Structures with Nuclear Backscattering and X-ray Diffraction," J. Vac. Science and Technol, 11, 86 (1974).

10. H. Kräutle, W. K. Chu, M-A. Nicolet, J. W. Mayer and K. N. Tu, "Reaction of Thin Metal Films with a SiO_2 Substrate," Proceedings of the International Conference on Applications of Ion Beam to Metals, Albuquerque, N. Mexico, Plenum Press, New York 1974, p. 193.

11. T. H. DiStefano and M. Shatzkes, "Impact Ionization Model for Dielectric Instability and Breakdown," Appl. Phys. Lett. 25, 685 (1974).

12. E. I. Alessandrini, D. R. Campbell and K. N. Tu, "Surface Reaction on MOS Structure," J. Appl. Phys. 45, 4888 (1974).

13. K. N. Tu, E. I. Alessandrini, W. K. Chu, H. Kräutle, and J. W. Mayer, "Epitaxial Growth of Nickel Disilicide on Silicon," Japan J. of Appl. Phys., Suppl. 2, Part 1, 669 (1974).

14. W. K. Chu, H. Kräutle, J. W. Mayer, H. Müller, M-A. Nicolet and K. N. Tu, "Identification of the Dominant Diffusing Species in Silicide Formation," Appl. Phys. Lett. 25, 454 (1974).

15. W. K. Chu, S. S. Lau, J. W. Mayer, H. Müller and K. N. Tu, "Implanted Noble Gas Atoms as Diffusion Markers in Silicide Formation," Thin Solid Films 25, 393 (1975).

16. K. N. Tu, W. K. Chu and J. W. Mayer, "Structure and Growth Kinetics of Ni_2Si on Si," Thin Solid Films 25, 403 (1975).

17. T. H. DiStefano and M. Shatzkes, "Dielectric Instability and Breakdown in Wide Bandgap Insulators," J. Vac. Sci. & Tech., 37 (1975).

18. K. N. Tu, "Selective Growth of Metal-Rich Silicide of Near Noble Metals," Appl. Phys. Letters, 27, 221 (1975).

19. J. W. Mayer, J. M. Poate and K. N. Tu, "Thin Film and Solid Phase Reactions--Traffic in the Submicron World," Science, Oct. (1975).

20. T. H. DiStefano and J. M. Franz, "Electronic Structure of Deep Traps in SiO_2-Si_3N_4 by Photodepopulation Spectroscopy," to by published in 4th Annual Symposium on Analytic Techniques for Semiconductor Surfaces, NBS (1975).

21. T. H. DiStefano, "Photoemission and Photovoltaic Imaging of Semiconductor Surfaces," to be published in 4th Annual Symposium on Analytic Techniques for Semiconductor Surfaces, NBS (1975).

22. J. W. Philbrick and T. H. DiStefano, "Scanned Surface Photovoltage Detection of Defects in Silicon Wafers," to be published in IEEE Transactions on Reliability Physics, (1975).

23. C. G. Wang and T. H. DiStefano, "Intrinsic Polarization at Metal-Insulator Interfaces," to be published in the Prodeedings of the 2nd Annual Conf. on the Physics of Compound Semiconductor Interfaces, CRC Critical Reviews, (1975).

24. J. L. Freeouf and D. E. Eastman, "Photoemission Measurement of Filled and Empty Surface States on Semiconductors and Their Relation to Schottky Barriers," Phys. Rev. in press.

25. Z. A. Weinberg and R. A. Pollak, "Hole Conduction and Valence Band Structure of Si_3N_4 Films on Si," Appl. Phys. Lett. Aug. 15 (1975).

26. K. N. Tu, D. R. Campbell, E. I. Alessandrini and S. Libertini, "Surface Reaction on MOS Structures - II", submitted to J. of Appl. Phys.

27. J. E. Baglin, K. N. Tu and T. H. DiStefano, "Densification of Amorphous SiO_2 by Exposure to an Ion Beam", submitted to J. of Appl. Phys.

28. T. H. DiStefano and M. Shatzkes, J. Vac. Sci. Technol. 13, 50 (1976).

Oral Presentations under F19628-73-C-0006
and F19628-74-C-0077

1. T. H. DiStefano, "Impurity Induced Dielectric Breakdown in SiO_2," AVS National Symposium, Chicago, 5 Oct. 1972.

2. D. R. Campbell, E. I. Alessandrini, K. N. Tu and J. E. Lewis "Phosphorus Diffusion and Catalyzed Crystallization in Amorphous Films of SiO_2," Electrochemcial Society Meeting, Miami Beach, Oct. 8-13, 1972.

3. K. N. Tu, Chairman of the Session on Advances in Amorphous to Crystalline Phase Transformation, 1972 Materials Engineering Congress, Cleveland, Oct. 14-19, 1972.

4. K. N. Tu, "Interdiffusion in Thin Films," (Invited) Dept. of Electrical Engineering, Caltech, Pasadena, California, Nov. 13, 1972.

5. T. H. DiStefano, "Electrical Interfaces," (Invited), Princeton Univ., Nov. 20, 1972.

6. T. H. DiStefano hosted an AVS regional symposium on "Electrical Properties of Material Interfaces," at IBM Yorktown Heights, December 7, 1972. His paper entitled, "Alteration of Electronic Barriers," was presented.

7. T. H. DiStefano, "Electronic Interfaces," (Invited) ECS, Ottawa, January 19, 1973.

8. T. H. DiStefano, "Electronic Interfaces," (Invited), Yale Univ. January 26, 1973.

9. T. H. DiStefano, "Gross Inhomogeneities in the Quasi-Classical Fermi Gas," APS Meeting, New York, January 29, 1973.

10. T. H. DiStefano and R. B. Laibowitz, "Photoemission Study of Niobium Glass Films," APS Meeting, New York, February 1, 1973.

11. E. I. Alessandrini, D. R. Campbell, "Catalyzed Crystallization and Transformation in SiO_2 Thin Films," ITL Meeting on Thin Film and Coating Technology, IBM Res. Center, February 7-9, 1973.

12. R. B. Laibowitz, P. Chaudhari, S. Herd, and S. Mader, "Direct Observation of Structural Changes in Switchable Materials," APS Meeting, San Diego, March 21, 1973.

13. T. H. DiStefano, "Thermionic Emission into Insulating SiO_2," APS Meeting, San Diego, March 21, 1973.

14. K. N. Tu, J. F. Ziegler and C. J. Kircher, "Interaction of V with Thermally Grown SiO_2," Materials Engineering Congress, Chicago, October 1-4, 1973.

15. J. W. Mayer and K. N. Tu, "Analysis of Thin Film Structures with Nuclear Backscattering and X-ray Diffraction," (Invited) 20th National Vac. Symp., New York October 9-12, 1973.

16. T. H. DiStefano, P. K. Roy, and M. Shatzkis, "Dielectric Breakdown and Radiation Effects in SiO_2," Fourth Intern. Silicon Interface Specialists Conf. San Juan, December 10, 11, 1973.

17. J. Franz and T. H. DiStefano, "Electronic Structure of the SiO_2-Si_3N_4 Interface," Fourth Intern. Silicon Interface Specialities Conf. San Juan, December 10, 11, 1973.

18. T. H. DiStefano, "UV Photoemission and Scanning Internal Photoemission Measurements for Thin Film and Interface Studies," Gordon Conf. on Thin Films and Solid Surfaces, Santa Barbara, January 24, 1974 (Invited).

19. T. H. DiStefano, "Photoinjection Study of Hot Electron Scattering in LiF." December 1973.

20. R. K. Roy and T. H. DiStefano, "Optical Properties of Various Allotropes of SiO_2," The March Meeting of the American Physical Society, Philadelphia, March 25-28, 1974.

21. E. I. Alessandrini, D. R. Campbell and K. N. Tu, "Surface Reactions on MOS Structures," ACA Spring Meeting at the University of California (Berkeley) March 25-29, 1974.

22. W. K. Chu, H. Kräutle, J. W. Mayer, M-A. Nicolet and K. N. Tu, "Use of Xe Markers to Identify Diffusing Species in Silicide Formation," APS 1974 March Meeting, Philadelphia, Penna., March 27, 1974.

23. K. N. Tu, E. I. Alessandrini, W. K. Chu, H. Kräutle and J. W. Mayer, "Epitaxial Growth of Nickel Disilicide on Silicon," The 6th International Vacuum Congress, Kyoto, Japan, March 20, 1974.

24. K. N. Tu, "Silicide Formation by Contact Reaction," (Invited) AVS Greater New York Chapter 1974 Symposium on Contact Reaction, Hoboken, New Jersey, April 24, 1974.

25. K. N. Tu, "Silicide Formation By Contact Reaction," (Invited) Tsing Hwa University, Hsin Chu, Taiwan, Rep. of China, April 2, 1974.

26. T. H. DeStefano "Interface Polarization Layers," (Invited) AVS Symposium on "Electronic and Structural Properties of Interfaces," RCA, Princeton, June 5-6, 1974. T. H. DiStefano co-chaired the symposium.

27. W. K. Chu, S. S. Lau, J. W. Mayer, H. Müller and K. N. Tu, "Implanted Noble Gas Atoms as Diffusion Markers in Silicide Formation," International Conference on "Low Temperature Diffusion and Applications to Thin Films" August 12-14, Yorktown Heights, New York, 1974.

28. K. N. Tu, W. K. Chu and J. W. Mayer, "Structure and Growth Kinetics of Ni_2Si on Silicon," Intern. Conf. on "Low Temperature Diffusion and Applications to Thin Films," August 12-14, 1974, Yorktown Heights, New York.

29. T. H. DiStefano, "Structure and Chemistry of Silicon and Silicon Dioxide Interfaces by Optical Scanning," (Invited) August 19, 1974, Burlington vermont.

30. K. N. Tu, "Silicide Formation by Contact Reaction," (Invited) August 2, 1974, Comsat Lab., Clarksburg, Maryland.

31. T. H. DiStefano, "Dielectrics, Reliability, and Interfaces," AFCRL, Lexington, Mass., November 18, 1974.

32. T. H. DiStefano, "Dielectric Instability and Breakdown in Wide Bandgap Insulators," (Invited) AVS National Symposium in Anaheim, CA, October 8-11, 1974.

33. T. H. DiStefano and K. N. Tu, "The Physics of Interface Interactions," ARPA Surface Science Colloquium, December 10,11, 1974, University of Pennsylvania.

34. T. H. DiStefano, Panel Review of ARPA funded research on Surface Science, ARPA National Symposium on Surface Science, December 4-6, 1974, University of Pennsylvania.

35. C. G. Wang and T. H. DiStefano, "Intrinsic Polarization Layer for Metal-Insulator Interfaces." 2nd Annual Conference on the Physics of Compound Semiconductor Interfaces, February 4-6, 1975, UCLA, LA, California.

36. T. H. DiStefano, (Invited) "Photovoltaic Imaging of the Semiconductor-insulator Interface," 2nd Annual Conference on the Physics of Compound Semiconductor Interfaces, February 4-6, 1975 UCLA, LA, California.

37. D. E. Eastman and J. L. Freeouf (Invited) "Photoemission Measurements of Filled and Empty Surface States on Semiconductors and Their Reaction to Metal-Semiconductor Barrier Energies," 2nd Annual Conf. on the Physics of Compund Semiconductor Interfaces, UCLA, LA, California, February 4-6, 1975.

38. B. Fischer, R. A. Pollak, T. H. DiStefano, and W. D. Grobman, "The Electronic Structure of $Si_xGe_{1-x}O_2$ from Photoemission Spectroscopy," American Physical Society Meeting - Denver, Colorado, March 31-April 3, 1975.

39. P. K. Roy, R. A. Pollak, T. H. DiStefano, and W. D. Grobman, "The Structure of SiO_2 Polymorphs by S-Ray Photoelectron Spectroscopy," American Physical Society Meeting - Denver, Colorado, March 31-April 3, 1975.

40. T. H. DiStefano, (Invited), "Interface Polarization," American Physical Society Meeting, March 31-April 3, 1975, Denver, Colorado.

41. T. H. DiStefano (Invited) "Dielectric Breakdown in Wide Bandgap Insulators," in the Solid State Seminar at Stanford University, February 7, 1975.

42. T. H. DiStefano, (Invited), Photoemission and Photovoltaic Imaging of Semiconductor Surfaces," NBS Workshop on Surface Analytic Techniques IV, Gaithersburg, April 23-24, 1975.

43. T. H. DiStefano served on the Program Committee for the 2nd Annual Conference on the Physics of Compund Semiconductors.

44. D. E. Eastman (Invited) "Empty Semiconductor Surface States: Adsorbate Effects and the Metal-Semiconductor Interface," at Bell Telephone Labs., May 9, 1975.

45. K. N. Tu. (Invited) "Silicide Formation by Contact Reactions," at the Department of Electrical Engineering, Caltech., Pasadena, California on April 28, 1975.

46. K. N. Tu (Invited) "Silicide Formation by Contact Reactions," at the Electrochemical Society Spring Meeting, Toronto, Canada, on May 14, 1975.

47. K. N. Tu chaired a session on "Thin Films and Implantation," at the Electrochemical Society Spring Meeting, Toronto, Canada, May 11-15, 1975.

48. T. H. DiStefano "Scanned Surface Photovoltage Images of Defects on Semiconductors," at the Device Research Conference, Ottawa, Canada, June 24-26, 1975.

49. T. H. DiStefano and J. M. Franz, "Electronic Structure of Deep Traps in SiO_2-Si_3N_4 by Photodepopulation Spectroscopy," NBS Workshop on Surface Analytic Techniques IV, Gaithersburg, April 23-24, 1975.

50. K. N. Tu organized a two-day symposium on "Interfacial Reactions in Solids," held at Cincinnati, Ohio, November 11-12, 1975.

51. K. N. Tu (Invited) "Metal-Semiconductor Interaction" Symposium on "Interfacial Reactions in Solids", Cincinnati, Ohio, Nov. 11-12, 1975.

52. K. N. Tu (Invited) "Kinetics of Silicide Formation" Gordon Conference on "Thin Films and Solid Surfaces" Andover, New Hampshire, Aug. 18-22, 1975.

MISSION
of
Rome Air Development Center

RADC plans and conducts research, exploratory and advanced development programs in command, control, and communications (C^3) activities, and in the C^3 areas of information sciences and intelligence. The principal technical mission areas are communications, electromagnetic guidance and control, surveillance of ground and aerospace objects, intelligence data collection and handling, information system technology, ionospheric propagation, solid state sciences, microwave physics and electronic reliability, maintainability and compatibility.

Printed by
United States Air Force
Hanscom AFB, Mass. 01731